

# 3D reconstruction of the *Lapis Tiburtinus* (Tivoli, Central Italy): The control of climatic and sea-level changes on travertine deposition

Alessandro Mancini<sup>1</sup>  | Giovanna Della Porta<sup>1</sup>  | Rudy Swennen<sup>2</sup>  | Enrico Capezzuoli<sup>3</sup> 

<sup>1</sup>Department of Earth Sciences "A. Desio", University of Milan, Milan, Italy

<sup>2</sup>Geology, Department of Earth and Environmental Sciences, KU Leuven, Heverlee, Belgium

<sup>3</sup>Department of Earth Sciences, University of Florence, Florence, Italy

## Correspondence

Alessandro Mancini, Department of Earth Sciences, University of Milan, via Mangiagalli 34, 20133 Milan, Italy.  
Email: [alessandro.mancini@unimi.it](mailto:alessandro.mancini@unimi.it)

## Funding information

This work was supported by the TraRas project, financed by Shell, Total and Petrobras. The borehole cores were donated by Equinor ASA to Giovanna Della Porta (University of Milan)

## Abstract

3D modelling is a fundamental tool to visualize and understand the history of sedimentary basin filling and to reconstruct the geobody architecture. Spatial distribution of discontinuity surfaces and geobody characteristics provide valuable information on the factors controlling the sedimentary evolution of basins. Several Neogene-Quaternary basins of central-western Italy are controlled by extensional and strike-slip tectonics and characterized by travertine deposition, related to hydrothermal fluids rising up along discontinuities and fractured carbonate bedrocks. This study presents the 3D modelling results of the quarry area within the tectonically controlled Acque Albule Basin (Tivoli, Central Italy) that hosts the Pleistocene *Lapis Tiburtinus* travertine. The 3D reconstruction of the different surfaces bounding the travertine units shows a complex architecture composed of depressions, reliefs and channels as predominant morphological elements related to four different depositional environments (subaqueous, palustrine, slope and travertine channel). The reconstructed surface maps highlight the presence of laterally migrating, E–W-oriented lens-shaped geometries, with a drainage system persistent through time oriented towards the southern part of the study area in the direction of the Aniene River, bordering the Acque Albule Basin in the South. The *Lapis Tiburtinus* travertine developed in an area of 28 km<sup>2</sup>, accumulated in a system composed of sub-basins (approximately 1–2 km<sup>2</sup> wide) with subaqueous conditions interconnected by a hydrographic network, controlled through time by fluctuations of the Aniene River base level. Based on the results obtained, base-level fluctuations of the Aniene River, related to glacio-eustatic sea-level oscillations of the last 115 kys associated with alternation of humid and arid climatic conditions, arise as the most important factor affecting the architecture of the travertine geobodies.

## KEYWORDS

3D modelling, base-level fluctuations, Central Italy, climate changes, *Lapis Tiburtinus*, Pleistocene, travertine

This is an open access article under the terms of the Creative Commons Attribution License, which permits use, distribution and reproduction in any medium, provided the original work is properly cited.

© 2021 The Authors. *Basin Research* published by International Association of Sedimentologists and European Association of Geoscientists and Engineers and John Wiley & Sons Ltd.

### Highlights

- Travertine deposits develop in continental basin;
- 3D modelling allows defining the architecture of travertine geobodies;
- Climatic and sea-level changes with tectonic activity are the most important factors controlling travertine evolution and deposition.

## 1 | INTRODUCTION

Sedimentary basins form in diverse geological settings with different subsidence regimes creating accommodation filled by sediments (Allen & Allen, 2008). Subsidence and accommodation creation can be driven by different factors, as thinning of crust, volcanic activity, tectonic loading or changes in lithosphere thickness (Dickinson, 1993). The study of sediment fills and the architecture of sedimentary units provides information about the history and sedimentary evolution of basins (Lerche, 1990).

3D modelling allows characterizing the architecture of sedimentary basins. Such approach addresses the vertical and lateral relationships of depositional systems defining the different sedimentary 'building blocks' (geobodies) and their spatial distribution. Geobodies display different scales of architectural units, as well as geometries and bounding surfaces, which are related to sedimentary processes and the extrinsic and intrinsic controlling factors leading to their formation and superposition through space and time.

Travertine deposits show complex facies distributions due to the numerous extrinsic (e.g. underlying substrate morphology and topographic gradient, fault patterns and tectonic setting, hydrogeology and geometry of the springs and climate) and intrinsic (interaction between biological and physico-chemical processes) factors affecting their deposition and evolution (Della Porta, 2015; Guo & Riding, 1998; Jones & Renaut, 1995; Pentecost, 2005; Shiraishi et al., 2020). The relationship between travertine deposition and tectonic activity is well demonstrated in the published literature (Brogi et al., 2010, 2018). Pleistocene glacial and interglacial climatic fluctuations, characterized at temperate latitudes by alternation of cold-arid and warm-humid conditions, respectively, were able to influence water supply that fed the springs, due to the fluctuations in rain precipitations (Pedley, 1990). For this reason, travertine distribution is directly influenced by the quantity of groundwater available in the aquifers. This extrinsic phenomenon is able to influence geobody architectures and facies characteristics, according to many authors (Capezzuoli et al., 2014; Guo & Riding, 1999; Jones & Renaut, 1995).

Different depositional models, influenced by extrinsic and intrinsic parameters, are reported in the literature both for ambient-temperature calcareous tufa and for hydrothermal travertine (related to thermal water springs; thermogene travertine sensu Pentecost, 2005; travertine sensu Capezzuoli et al., 2014), based on sedimentological analysis and rarely on 3D modelling at basin scale (Anzalone et al., 2017; Chafetz & Folk, 1984; Chafetz & Guidry, 1999; Claes et al., 2015; Croci et al., 2016; D'Argenio et al., 2008; Della Porta, 2015; Della Porta, Capezzuoli, et al., 2017; Della Porta, Croci, et al., 2017; Erthal et al., 2017; Folk et al., 1985; Guo & Riding, 1994, 1998, 1999; Jones & Renaut, 1995; Pentecost, 2005). In this study, a 3D model of travertine deposits (*Lapis Tiburtinus*) hosted in the Acque Albule Basin (Tivoli, Central Italy, Pleistocene) is presented. The term 'travertine' is derived from the Italian *travertino*, coming from the Latin *Lapis Tiburtinus*, meaning 'stone of Tibur' (Chafetz & Folk, 1984) that was the Roman name for the present-day town of Tivoli, located nearly 20 km east of Rome (Central Italy) along the Aniene River (Chafetz & Folk, 1984; Della Porta, Croci, et al., 2017; Faccenna et al., 2008).

The Acque Albule is part of the Roman Basin (Gelasian; Milli et al., 2016). This area was affected largely by continuous regional uplift, intense volcanic activity and glacio-eustasy fluctuations (De Rita et al., 1993, 1995; Fornaseri, 1985; Karner et al., 2001; Mancini et al., 2007; Peccerillo, 2005). The Roman Basin is crossed by the Tiber River and its tributaries, such as the Aniene River (Giustini et al., 2020).

The Acque Albule Basin, representing the focus of this study, is considered, according to Faccenna et al. (2008), De Filippis, Anzalone, et al. (2013) and De Filippis, Faccenna, et al. (2013), a pull-apart basin, controlled by the activity of extensional faults (NW-striking) accompanied by transverse (NE-striking) or oblique (N-striking) strike-slip faults. According to De Filippis, Anzalone, et al. (2013) and De Filippis, Faccenna, et al. (2013), these structures have also influenced the latest stages of volcanism, while the N-S right-lateral strike-slip fault controls the hydrothermal outflows and the springs activity. The evolution of the entire Acque Albule Basin was largely controlled by tectonic activity, leading to creation of accommodation, with climate changes able to influence the groundwater circulation (Faccenna et al., 2008).

This study presents a detailed evaluation of the Acque Albule Basin travertine deposits, based on geological survey, line drawing on photo panels, correlation of stratigraphic logs and borehole core descriptions. The different geobodies composing the travertine deposits, as well as their bounding surfaces, were reconstructed following the concepts of synthem stratigraphy proposed by Chang (1975) as Unconformity-Bounded Stratigraphic Units (UBSUs).

The performed 3D models and the reconstructed bounding surface maps highlight the architecture of travertine

deposits hosted in the Acque Albule Basin, mainly developed in a system composed of depression and channel morphologies, laterally migrating during the last 115 kys.

The aim of this study is to provide a depositional model for the Pleistocene travertine deposits of the Acque Albule Basin, where the base-level fluctuations of the Aniene River, because of the relative sea-level oscillations driven by glacio-eustasy, probably controlled and influenced the geometries of the different travertine units and the evolution of the architecture of the basin sedimentary filling. In this view, the presented hypothesis, supported by quantitative data and 3D modelling of stratigraphic architecture, proposes that accommodation for the *Lapis Tiburtinus* travertine within the Acque Albule Basin was related to base-level fluctuations and the erosional activity of the Aniene River fluvial system, suggesting that the travertine architecture evolved in this case largely under the control of eustatic and climatic fluctuations during alternating glacial–interglacial phases.

## 2 | GEOLOGIC SETTING

### 2.1 | Regional setting. The Acque Albule Basin

The Acque Albule Basin is part of the Roman Basin (Conato et al., 1980; Della Porta, Croci, et al., 2017; Faccenna et al., 2008) and is confined by the Neogene Apennine fold and thrust belt to the North and to the East (i.e. Cornicolani-Lucretili and Tiburtini Mountains), by the Pleistocene quiescent volcano of the Colli Albani complex and the Aniene River to the South and, to the West, by the Tiber River valley, formed during the Pliocene-Quaternary extensional tectonics (De Filippis, Faccenna, et al., 2013) (Figure 1a,b).

Mesozoic-Cenozoic carbonates characterize the Apennine orogenic belt (Barchi, 2010; Patacca et al., 1992), organized in thrust sheets with piggy-back sequence, developed during the late Miocene-Pliocene time on the eastern (Adriatic Sea) side (Figure 1a,b). The western (Tyrrhenian Sea) side is instead considered affected by an extensional regime since the middle Miocene-Pliocene time linked to the opening of the Tyrrhenian Sea as a back-arc basin (Acocella & Funiciello, 2006; Chiodini et al., 2004; Funiciello et al., 1976; Mancini et al., 2014; Rossetti et al., 2007).

Located west of the town of Tivoli, the Acque Albule Basin is a depression with a gentle inclination from North to South and from East towards the West (Figure 1b and Figure S1). The local topography is characterized by a flat surface (average elevation of 50 m), gently inclined towards the southern part (with nearly 30 m of elevation in the southern part of the basin), in proximity of the Aniene River, with small reliefs (elevation between 80 and 70 m) in the central and northern part (see Figure S1). This depression

about 28 km<sup>2</sup> wide (De Filippis, Anzalone, et al., 2013; De Filippis, Faccenna, et al., 2013; Di Nezza et al., 2015; Faccenna et al., 2008) is characterized by moderate subsidence (0.4 mm/yr; De Filippis, Anzalone, et al., 2013; De Filippis, Faccenna, et al., 2013). Evidence of Pleistocene-Holocene tectonic activity (Faccenna et al., 2008) is locally highlighted by N-S-striking right-lateral and transtensional to normal faults inducing low seismicity (Billi et al., 2006; Corrado et al., 1992; Cosentino & Parotto, 1986; De Filippis, Anzalone, et al., 2013; De Filippis, Faccenna, et al., 2013; Faccenna et al., 1994, 2008; Gasparini et al., 2002).

### 2.2 | The *Lapis Tiburtinus* travertine

The Acque Albule Basin was filled by Plio-Pleistocene alluvial, lacustrine and epivolcanic succession, resting unconformably on Meso-Cenozoic (Figure 1d) marine carbonate succession corresponding to the local bedrock (De Rita et al., 1995; La Vigna et al., 2013a, 2013b). The top of this sedimentary succession is characterized by the presence of the *Lapis Tiburtinus* travertine, one of the largest (about 28 km<sup>2</sup> wide; Faccenna et al., 2008) and thickest (90 m; Faccenna et al., 2008) exposed travertine deposits of the world, developed during the Late Pleistocene (115–30 ka; Faccenna et al., 2008). The travertine deposits consist of sub-horizontal to bedded units, gently-dipping towards the South, East and West with onlapping geometries on the underlying erosional surfaces with variable thickness of 7–10 m, separated by erosional surfaces generally marked by thin soil (less than 1 m) deposits and pockets of conglomerate (De Filippis, Anzalone, et al., 2013; De Filippis, Faccenna, et al., 2013).

### 2.3 | Hydrogeology of the Acque Albule Basin

The hydrogeological regime of the Acque Albule Basin (Figure 1d) is influenced by: (i) the carbonate relief recharge area to the North, Northeast and East of the basin (Lucretili-Tiburtini and Cornicolani Mountains; Carucci et al., 2012; La Vigna et al., 2013a, 2013b) and by (ii) the presence of N-S striking faults and associated damage zones (Billi et al., 2006). According to La Vigna et al. (2013a, 2013b) and Carucci et al. (2012), the local groundwater flow conceptual model is characterized by three main hydrostratigraphic units. The first one is confined within the limestone-bedrock cropping out along the margins of the basin, where it is lowered by normal faults. The second, at the top of the bedrock, is located in the Pliocene sandy clayey marine deposits. At the top of the succession, the third aquifer is defined by the fractured travertine, strongly depleted by quarry and industrial activities. Pliocene deposits may be considered non-continuous

aquiclude. The mixed groundwater in the travertine partially flows from the hydrothermal springs and partially follows the flow path, in the direction of the Aniene River.

Many hydrothermal springs are located in the basin plain at the western boundary of the Apennine (De Filippis, Anzalone, et al., 2013; De Filippis, Faccenna, et al., 2013),

with various discharge volumes up to 4,000 L/s (Brunetti et al., 2013; Capelli et al., 1987; Carucci et al., 2012; Di Salvo et al., 2013; La Vigna et al., 2013b). The most important hydrothermal springs are located in the central part of the Acque Albule Basin (Regina Lake discharging ca. 1,850 L/s and Colonnelle Lake with ca. 250 L/s and temperature of ca.

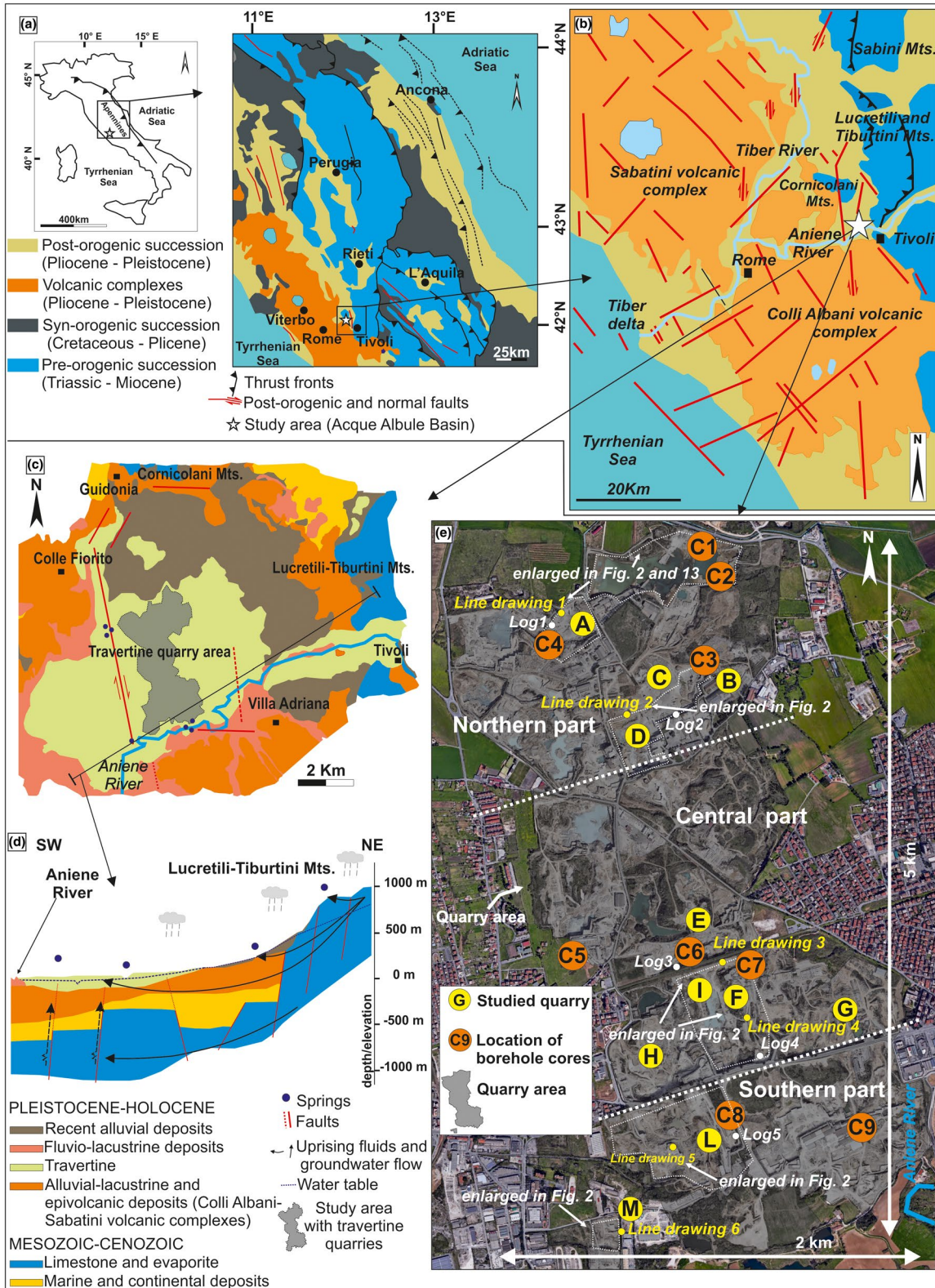


**FIGURE 1** (a) Geological map of Central Italy and (b) a detail of the study area. Central Italy is characterized in the eastern part by the fold and thrust Apennine orogenic belt, comprising fractured Meso-Cenozoic limestone and evaporite. The western sector, affected by extensional tectonics, including Tuscan, Latium and Campanian districts, is characterized by (i) reduced thickness of the lithosphere, (ii) high heat flow (Chiodini et al., 2004; Funiciello et al., 1976) and (iii) presence of numerous Pliocene-Quaternary sedimentary basins (Mancini et al., 2014; Milli et al., 2016) and magmatic districts (Acocella & Funiciello, 2006; Rossetti et al., 2007) (redrafted and modified after Bigi et al., 1990; Della Porta, Croci, et al., 2017; De Rita et al., 1995, 2002; Gaeta et al., 2000; Karner et al., 2001; Minissale, 2004; Vignaroli et al., 2019). (c) Geological map of the study area with indication of major faults and springs present in the area. Notice that the springs are located in proximity to the major structural features. (d) Hydrogeological model proposed for the travertine hosted in the Acque Albule Basin (modified after Carucci et al., 2012). (e) The study area with the location of the investigated quarries, studied boreholes, stratigraphic logs and the line drawings performed (modified from Google Earth; Digital Globe, 2018)

23°C, pH 6.0–6.2; Carucci et al., 2012; Di Salvo et al., 2013; La Vigna et al., 2013a; Minissale, 2004; Minissale et al., 2002; Pentecost & Tortora, 1989). They are located close to the N-S-striking, right-lateral, seismically active fault (Faccenna et al., 2008). The Aniense River represents the main runoff destination of all the thermal-superficial basin waters (La Vigna et al., 2013b).

## 2.4 | Previous depositional models of the *Lapis Tiburtinus* travertine

The *Lapis Tiburtinus* travertine deposits were studied by several authors starting from the 1980s. Chafetz and Folk (1984) suggested that this travertine succession developed in a lacustrine system, because of the presence of extensive and laterally continuous horizons, sometimes affected by karstic features, linked to periodic drainages of the lakes. Depositional systems, varying from sub-horizontal pools and dammed-terraces fed by vents to lakes up to low-angle spring cones, were reported by Pentecost (2005). Most of these interpretations were based on sedimentological observations of quarry walls without lateral stratigraphic correlations.

According to Faccenna et al. (2008), the *Lapis Tiburtinus* travertine deposits accumulated between 115 and 30 ka (Late Pleistocene) and the 70% in volume of the travertine deposited inside the Acque Albule Basin originated from thermal water springs (De Filippis, Anzalone, et al., 2013; De Filippis, Faccenna, et al., 2013). The travertine deposits were interpreted as a tabular plateau made of sub-horizontal benches, separated by erosional surfaces, with a progradational pattern and southward steepening of the strata (Faccenna et al., 2008). De Filippis, Anzalone, et al. (2013), De Filippis, Faccenna, et al. (2013) used the term travertine plateau to identify a large and massive thermal travertine deposit consisting of bedded travertine filling a tectonic depression and producing no prominent topography. The depocentre, with maximum thickness up to 80–90 m, coincided with a main N-S striking fault and the associated emergences of thermal water (Faccenna et al., 2008). Five sub-horizontal units, characterized by tabular geometries, with progradational

pattern towards the southern part, were identified in the *Lapis Tiburtinus* travertine.

These units are separated by erosional surfaces, controlled by episodic fluctuations of the water table influenced by Pleistocene palaeoclimate oscillations, nearby volcanic activity and fault-related deformation (De Filippis, Faccenna, et al., 2013; Faccenna et al., 2008).

According to the model proposed by De Filippis, Anzalone, et al. (2013), De Filippis, Faccenna, et al. (2013), the rise of thermal water and the discharge at the spring are considered main factors keeping open the fractured conduits that fed the travertine deposits. The high pressures of thermal water thus have promoted a two-fold effect: (1) the opening of pathways for the ascension of large volumes of geothermal fluids and (2) the subsidence of the basin. These processes must have led to a well-fed and subsiding geothermal lake where the travertine plateau grew for about 100,000 years with an associated depositional rate of 0.4 mm/yr. In particular, the large amount of water discharge caused the precipitation of calcium carbonate deposits also far away from the geothermal springs, hence driving the lateral progradation of the travertine plateau and its large volume (De Filippis, Anzalone, et al., 2013; De Filippis, Faccenna, et al., 2013).

Anzalone et al. (2017) reported on a 30 m-thick borehole core drilled in the NW of the quarry area, and interpreted the travertine as a deposit formed in a shallow lake and slope, characterized by the presence of numerous erosional discontinuities of different orders and magnitudes. Based on sedimentological, stratigraphic and geochemical data, Anzalone et al. (2017) proposed a cyclostratigraphic model of the travertine deposit and identified high-frequency cycles related to water table fluctuations and controlled by climatic changes driven by Milankovitch orbital forcing, sub-Milankovitch and millennial scale climatic cycles.

Erthal et al. (2017) focused on the travertine facies and distinguished six different shrub types, related to the depositional conditions, water flow hydrodynamics, CO<sub>2</sub> degassing rate, evaporation and influence of microbially mediated precipitation, with the entire *Lapis Tiburtinus* travertine succession related to subaqueous (extensive waterlogged flat setting) and slope depositional setting.

According to Della Porta, Croci, et al. (2017), travertine units are characterized by wedge-shaped geometry with variable lateral thickness (20–45 m thick), gently dipping and thinning towards the S, E and W. The travertine system was subdivided into three zones. The proximal depositional zone in the North, closer to the inferred active vents (N-NE parts of the area), was characterized by deposition in horizontal to gently dipping decametre-size pools belonging to a low-angle terraced system. The intermediate zone was characterized by a smooth to terraced slope setting with beds dipping 5°–40° southwards and eastwards. The distal zone in the South was interpreted as composed of lobes dipping southwards of smooth and terraced slope systems adjacent to marshes, alternating with alluvial-fluvial terrigenous deposits. The different unconformities, identifying 9 travertine units, were linked to erosional or non-depositional periods, suggesting that the travertine depositional system was controlled by the intermittent vent activity, changes in the location of the active vents, topographic gradient, rates of thermal water discharge and rates of carbonate precipitation.

### 3 | METHODS

Detailed and extended field observations (Figure 1e) were performed in different quarries located within the Acque Albule Basin, where the travertine succession is exposed for up to 45 m in thickness.

In the northern part of the study area, detailed stratigraphic logs and line drawings were performed in quarries A, B, C and D. Additional data were derived from C1, C2, C3 and C4 cored boreholes. In the central part, the same approach was used in quarries E, F, G, H and I, as well as derived from the different cored boreholes C5, C6 and C7. In the southern part of the study area, information is provided by the field survey done in quarries L and M and by the study of C8 and C9 cored boreholes.

The 37 measured stratigraphic logs were grouped in 5 logs representative of the different sectors studied integrated with 3 new borehole cores, reaching a maximum depth of 70 m. Measured logs were characterized sedimentologically and with regard to facies composition. These data were integrated with those presented in Erthal et al. (2017) and Della Porta, Croci, et al. (2017). The cored borehole studied by Anzalone et al. (2017) was not included due to the lack of precise location.

A total of 159 samples from the 3 new boreholes and outcrops were doubly impregnated with resin before thin section preparation due to the fragility of travertine, particularly at pore edges. A fluorescent dye was used to easily distinguish (micro)-porosity with fluorescent light microscope. The petrographic characterization was performed using an Olympus BX60 (Olympus Corporation, Tokyo, Japan) and a Leica (Leica Microsystems, Wetzlar, Germany) DM LP polarized light microscopes. A Zeiss Axio Imager Z1m. microscope with adapted filter set (EX BP365/12 EM LP397, EX G 365

EM LP 420 and EX BP 450-490 EM LP 515) was used to take pictures of the analysed samples.

Detailed photographs of the saw-cut quarry walls from the different excavation levels were printed and used in the field for detailed line drawings. These line drawings allowed assessment of the thickness and lateral continuity and distributions of the different lithofacies (Figure 2). Lithofacies descriptions, proposed by Della Porta, Croci, et al. (2017) and Erthal et al. (2017), were assembled to better characterize macro- and mega-scale units (geobodies). The different geobodies that characterize the entire travertine succession were identified based on observable and mappable bounding discontinuities, following the concept proposed by Chang (1975) and formalized by NACSN (1983) and Bhattacharya and Walker (1991), related to the allostratigraphy concept and based on the Unconformity Bounded Sedimentary Units (UBSUs; Chang, 1975). The UBSUs are stratigraphic units that allow a classification of sedimentary bodies in areas characterized by cyclical phenomena, as tectonically and climatically driven sea-level changes. In this view, the unconformity-bounded stratigraphic units (UBSUs) can be defined as units of rocks bounded by unconformity surfaces.

Geobody shapes and morphologies were modelled using the 3D software Google Sketchup 2017. Previously, a grid of 15 km<sup>2</sup> divided in rectangles of equal dimension of *X* (25.57 m) and *Y* (31.19 m) axis was modelled based on the major marker beds and unconformities recognized in the field and in the cored boreholes. Values of latitude and longitude of the different stratigraphic logs and cored boreholes are provided based on handheld GPS. For the non-visited quarries, modelling was integrated using available topographic maps of the area.

## 4 | RESULTS

### 4.1 | Lithofacies

The characterization and classification of the different deposits are presented in Figures 3 and 4, Tables 1 and 2, and subdivided into 'travertine' and 'terrigenous and volcanic deposits' lithofacies types.

#### 4.1.1 | Travertine lithofacies associations

Some of the here-reported lithofacies were previously detailed at macro- and micro-scale (cm-mm) by Erthal et al. (2017) and Della Porta, Croci, et al. (2017). Such descriptions are here combined to simplify and rationalize the lateral and vertical heterogeneities, typical of travertine deposits (cf. Guo & Riding, 1998). The different lithofacies

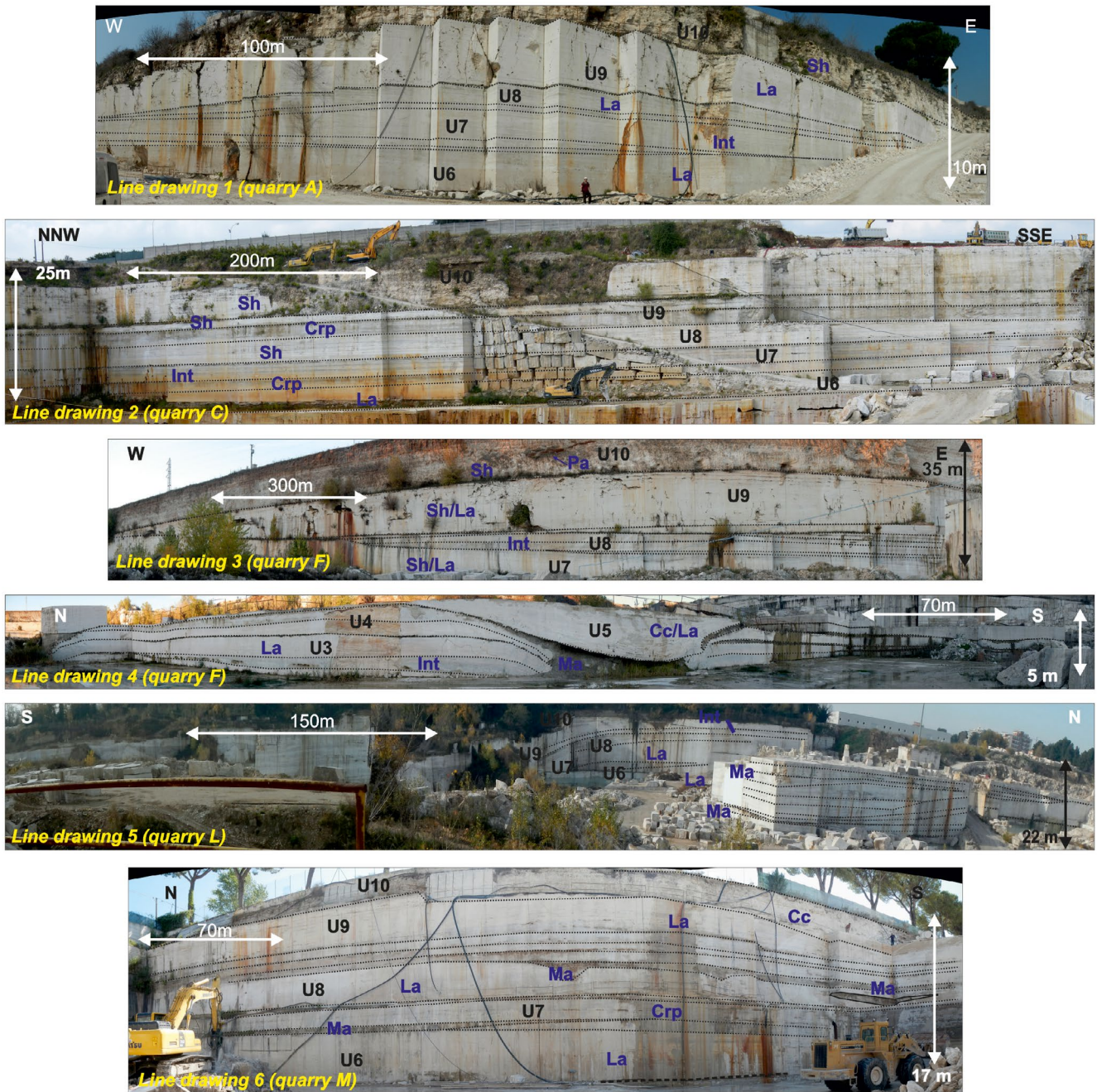


**FIGURE 2** Line drawings performed on the quarry walls in the travertine quarry area. The northern part of the travertine deposits is characterized by lenticular convex-upward and tabular geometries as illustrated in the line drawings 1 and 2. Lenticular concave-upward geometries, depressions filled by travertine deposits with different scales are typical of the central part of the deposits, as shown in line drawings 3 and 4. In the southern part of the travertine deposits, lenticular and tabular geometries occur, as in line drawings 5 and 6 (Sh: shrub; La: laminated deposit; Cc: crystalline crust; Int: intraclast deposit; Crp: coated reed and phytoclast; Pa: palaeosoil; Ma: claystone and marlstone deposits; U: unit). For the different units reported, see Figure 6

are interpreted with respect to the depositional environment as in previous studies on travertine (Anzalone et al., 2017; Chafetz & Folk, 1984; Chafetz & Guidry, 1999; Claes et al., 2015; Croci et al., 2016; D'Argenio et al., 2008; Della Porta, 2015; Della Porta, Capezzuoli, et al., 2017; Folk et al., 1985; Gandin & Capezzuoli, 2014;

Guo & Riding, 1994, 1998, 1999; Jones & Renaut, 1995; Pentecost, 2005).

*Shrub*

Shrub lithofacies (Figure 3a,a1,a2) association (including T2 clotted peloidal micrite dendrite boundstone, T3

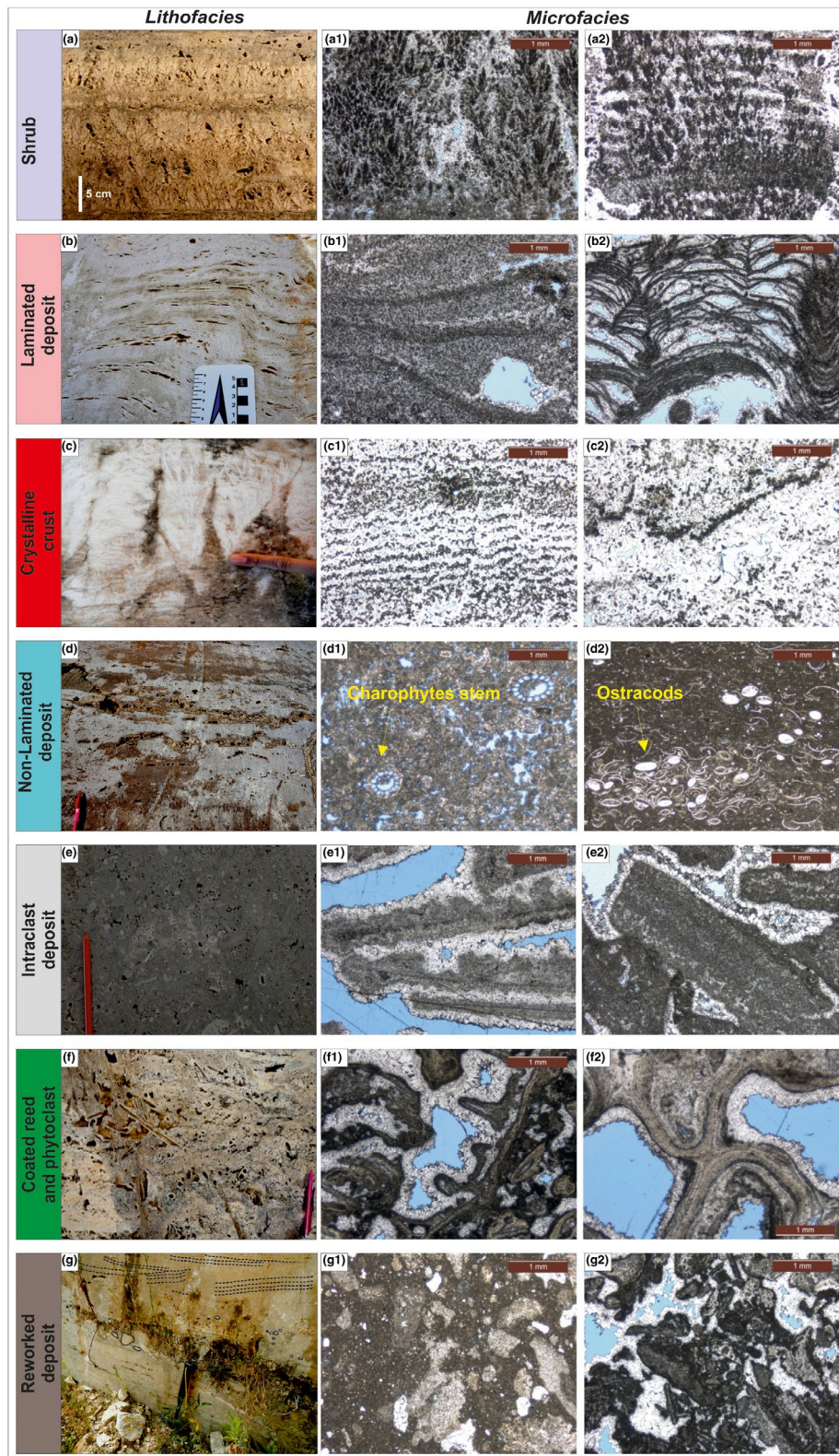


**FIGURE 3** Field photos and thin section images of the 7 lithofacies associations characterizing the travertine deposits. (a, a1, a2) Shrub lithofacies. (b, b1, b2) Laminated deposit lithofacies. (c, c1, c2) Crystalline crust lithofacies. (d, d1, d2) Non-laminated deposit lithofacies. (e, e1, e2) Intraclast deposit lithofacies. (f, f1, f2) Coated reed and phytoclast lithofacies. (g, g1, g2) Reworked deposit lithofacies



**TABLE 1** Description of the travertine lithofacies associations reported in Figure 3

Lithofacies	Description	Accessories	Depositional environments	Energy-process
Shrub	Clotted peloidal micrite dendrite boundstone	Coated grains, aggregates of clotted peloidal micrites, coated bubbles, rafts	Pools (shallow lake), ponds	Low. Biologically-influenced
Laminated deposit	Laminated micrite boundstone, mudstone, packstone	Coated grains, aggregates of clotted peloidal micrites, coated bubbles, rafts, intraclasts	Pools (shallow lake), ponds, slope	Medium, low, high-biologically-influenced
Crystalline crust	Crystalline fan dendritic cementstone and cruststone	Crystalline fans of calcite (cm-mm)	Slope, rims	High. Abiotic
Non-laminated deposit	Packstone, mudstone	Coated reed stems, <i>Charophytes</i> , gastropods, ostracods, intraclasts	Ponds with input of freshwater, Pools (shallow lakes)	Low. Biologically-influenced
Intraclast deposit	Floatstone, packstone, rudstone	Angular Intraclasts (cm-m)	Pools (?)	Medium, low. Selective transport
Coated reed and phytoclast	Phytothermal boundstone, phytoclastic packstone	Coated reed stems, <i>Charophytes</i> , gastropods, rafts	Distal part of ponds, environment affected by input of freshwater, pools (shallow lakes)	Low. Biologically-influenced
Reworked deposit	Packstone, rudstone	Well rounded Intraclasts and extraclasts (cm-mm) sometimes with imbrication and cross-bedding	Travertine channels	High. Selective transport

**TABLE 2** Description of the terrigenous and volcanic deposits lithofacies and reported in Figure 4

Lithofacies	Description	Accessories	Depositional environments	Energy
Palaeosoil	Immature brown palaeosoils rich in clay. Debris flow well cemented deposits brown or grey with clasts poorly sorted and rudstone with intraclasts	Intraclasts, bones, root moulds, gastropods	Pedogenized substrate	Medium low
Claystone and marlstone deposits	Clay, marl, silt	Pyrite, gastropods	Pools, ponds, shallow lake	Very low
Sand, sandstone and conglomerate	Polymictic and monomictic conglomerates with rounded and sub-rounded clasts. Grey-green sandstones with cross-bedding	Clasts of travertine and marine limestone of Lucretili and Tiburtini mountain ranges	Rivers, fluvial channel	High medium
Volcanic and volcaniclastic deposits	Pyroclastic flow and ash deposits, brown, grey and green (Colli Albani and Sabatini Volcanic complexes)	Lapilli, Leucite, Biotite, Phlogopite, Augite	–	–

micrite-microsparite crust boundstone, T4 coated gas bubble boundstone to wackestone, T6 radial coated grain grainstone and T7 raft grainstone/rudstone in Della Porta, Croci, et al., 2017) is one of the most abundant facies associations, with high lateral continuity over hundreds of square metres (Chafetz & Folk, 1984) and up to 40 m in thickness with tabular geometries. The shrub lithofacies association is generally lateral to and intercalated with the laminated deposit lithofacies association. The shrub lithofacies association is mainly characterized by 1- to 10-cm thick dendrites resembling

microbialite-like structures with domal and layered morphologies (Chafetz & Folk, 1984; Chafetz et al., 1991; Guo & Riding, 1998; Rainey & Jones, 2009). Petrographically, such lithofacies can be described as clotted peloidal dendrite boundstone with dark to grey sub-spherical micritic aggregates of 0.5–0.1 mm. The shrub lithofacies from the *Lapis Tiburtinus* travertine is interpreted to be deposited either in shallow lakes by many authors (Chafetz & Folk, 1984), pool environments fed by vents (Chafetz & Folk, 1984; Guo & Riding, 1994) or terraced systems on distal slopes (Faccenna

et al., 2008). Pleistocene travertine successions from Rapolano Terme in Tuscany (Central Italy) reflect a comparable setting where shrub lithofacies is interpreted to have formed in 'extensive waterlogged flats' (Guo & Riding, 1994, 1998). According to Erthal et al. (2017), the shrub lithofacies developed in slow to moderate energy flat and sub-horizontal ponds and pools of terraced slope systems, associated with limited flow and turbulence of thermal water.

#### *Laminated deposit*

Together with the shrub, the laminated deposit (Figure 3b,b1,b2) is the other most common lithofacies association. This association comprises the travertine lithofacies types labelled as T3 micrite-microsparite crust boundstone, T4 coated gas bubble boundstone to wackestone, T5 laminated boundstone, T6 radial coated grain grainstone and T7 raft grainstone/rudstone in Della Porta, Croci, et al. (2017). Laminated deposit lithofacies association forms tabular, concave or convex lenticular bodies, up to 40 m in thickness. Secondly, it occurs as centimetre–metre thick intercalations within the shrub lithofacies association but can also be present within the crystalline crust lithofacies. Petrographically, such lithofacies can be described as a fine laminated micrite boundstone with 0.2 mm sub-horizontal to slightly undulated lamination and appears mainly composed of dense to clotted peloidal micrite, vertically and laterally passing to coated grain layers. Generally, this laminated lithofacies is associated with microbial mat (Gandin & Capezzuoli, 2014), which can occur in sub-horizontal pools and ponds or in terraced or inclined slope surfaces associated with the fast-flowing crystalline crust lithofacies. Laminated lithofacies often occurs associated with shrub lithofacies, indicative of evaporative water (Folk et al., 1985; Gandin & Capezzuoli, 2014; Guo & Riding, 1998).

#### *Crystalline crust*

Crystalline crust lithofacies (Figure 3c,c1,c2) association reaches a maximum thickness of 10 m and is characterized by convex-upward, lenticular geometries with flank inclination up to 20°. Generally, this lithofacies association laterally passes to laminated deposit, shrub and intraclast deposit lithofacies types. At the macro scale, the crystalline crusts appear as laminated bands developed perpendicular to the substrate with variable sizes, ranging from centimetres to decimetres, erroneously interpreted as syn-sedimentary folds (Alçiçek et al., 2017). Petrographically, crystalline crust appears as vertical fans of dendritic crystals forming cementstone. The lozenge-shaped turbid, inclusion-rich crystals (100–600 µm long, 40–60 µm wide) depart from a central elongated crystal acting as a stalk (T1 crystalline dendrite cementstone in Della Porta, Croci, et al., 2017). The crystalline dendrite lithofacies

association occurs in high-energy, turbulent environments with fast-flowing sheets of thermal water running in variably steep sub-environments (smooth slopes, terraced slopes, pool rims and cascades; Gandin & Capezzuoli, 2014; Mancini et al., 2019; Rainey & Jones, 2009). Generally, crystalline crust develops on inclined steeply dipping surfaces of slopes with associated rims and walls of pools organized in terraced and micro-terraced, with rapid physico-chemical carbonate precipitation due to CO<sub>2</sub> degassing (Chafetz & Guidry, 1999; Della Porta, 2015; Della Porta, Capezzuoli, et al., 2017; Folk et al., 1985; Guo & Riding, 1998; Jones & Renaut, 1995). The thickness of crystalline crust layers is proportional to precipitation rates and thermal water flow velocity, whereas the growth lamination is attributed to periodic changes in water flow (Guo & Riding, 1998; Pentecost, 2005). On smooth slopes, the crystalline crust lithofacies occurs associated with T5 laminated boundstone and T6 radial coated grain grainstone facies described by Della Porta, Croci, et al. (2017).

#### *Non-laminated deposit*

This lithofacies (Figure 3d,d1,d2) association is characterized by plane parallel, sub-horizontal beds with maximum thickness of 5 m. It is always associated with coated reed and phytoclast lithofacies, frequently representing its lateral equivalent. Non-laminated lithofacies types resemble the laminated lithofacies in terms of texture and components, but are distinguished due to the lack of lamination (T10 clotted peloidal micrite grainstone/boundstone with *Charophytes* associated with T8 white coated reed boundstone to grainstone/rudstone in Della Porta, Croci, et al., 2017). Petrographically such lithofacies appears as mudstone, wackestone and packstone with amalgamated clotted peloidal micrite and intercalated with structureless micrite and microsparite. Gastropods, mould of plants (up to 1 cm long), ostracods, *Charophyte* stems (up to 5 mm long, 0.5 mm in diameter), and intraclasts (up to 1 mm) frequently occur. This lithofacies association is interpreted as accumulated in lacustrine–palustrine to stagnant pond environments or in shallow flat ponds, with occasional terrigenous and freshwater input, testified by the presence of ostracods and *Charophytes* (Della Porta, Croci, et al., 2017).

#### *Intraclast deposit*

This lithofacies association (Figure 3e,e1,e2) includes flat, laterally discontinuous beds of floatstone/wackestone, packstone, and rarely rudstone with reworked angular intraclasts (0.5–20 cm in size). The matrix is predominantly dark grey colour; erosional and subaerial exposure features are common such as fissures and cracks (labelled as T12 white intraclastic coated grain grainstone/rudstone and T13 grey intraclastic extraclastic wackestone/floatstone/rudstone in Della Porta, Croci, et al., 2017). A maximum of 2 m in thickness was measured

in the eastern portion of the study area. The geometries are generally tabular or lenticular concave-upward. Intraclast deposits pass laterally and vertically to all other travertine and terrigenous lithofacies (e.g. palaeosoils). According to Della Porta, Croci, et al. (2017), these deposits developed in pools or inclined surfaces associated with periods of subaerial exposure and travertine erosion due to interruption or deviation of thermal water flow. These beds are overlain by coated reeds encrusted when the thermal water flow resumed, according to Della Porta, Croci, et al. (2017). According to Faccenna et al. (2008), this lithofacies association suggests inactive periods of the hydrothermal system. Recently, Brogi et al. (2018) interpreted similar deposits, occurring in Rapolano Terme travertine, as soft sediment deformation structures (SSDS) triggered by earthquake events (seismites).

#### *Coated reed and phytoclast*

This lithofacies association (Figure 3f,f1,f2) is ubiquitous, with a maximum thickness of 2 m. It mostly shows concave-upward and convex-upward lenticular geometries, with lateral relationships with non-laminated lithofacies, secondarily with laminated deposit and shrub. It is formed by accumulation or lateral juxtaposition of cylindrical moulds, in growth position or as broken fragments (0.2–4 cm in diameter) of plant stems coated by grey to brown-orange micrite. *Charophytes* and gastropods frequently occur associated with plant moulds. Calcite coatings and subsequent decay of stems and/or plants that served as substrate for calcium carbonate precipitation are typical of this lithofacies association, which includes various lithofacies labelled as T8 white coated reed boundstone to grainstone/rudstone, T9 brown coated reed and *Charophytes* boundstone, T11 brown intraclastic phytoclastic packstone/grainstone/rudstone, T14 brown intraclastic phytoclastic packstone/grainstone to boundstone in Della Porta, Croci, et al. (2017). In agreement with Guo and Riding (1998), who studied similar lithofacies in the Terme di San Giovanni travertine system in Rapolano Terme (Italy), these lithofacies types occur in flat marshes and shallow lacustrine-palustrine environments with occasional subaerial exposure, suggesting climatic influence (freshwater input during rainy periods as referred by Guo & Riding, 1998) and/or distally cooled thermal waters (Della Porta, Croci, et al., 2017; Pedley, 1990).

#### *Reworked deposit*

Discontinuous, dark lenticular bodies (maximum 1.5 m thick) of packstone to rudstone/floatstone with moderately sorted and well-rounded to sub-angular (2–5 cm) intraclasts and extraclasts make up this lithofacies association (Figure 3g,g1,g2). Clasts locally show palaeocurrent imbrication with varying direction. Sedimentary bodies are characterized by erosional surfaces at the base, lenticular concave-upward geometry, laterally and vertically passing to all the other travertine lithofacies (mostly coated reed and

phytoclast and laminated deposits). Due to these characteristics, such lithofacies is attributed to a travertine channel environment. Similar deposits were described by Özkul et al. (2013), Brogi et al. (2010) and Guo and Riding (1999), respectively, in Turkey and in the Rapolano Terme (Italy) travertine deposits and generally located in the marginal part of shallow lacustrine environments, suggesting a fluvial influence on travertine depositional system.

#### 4.1.2 | Terrigenous and volcanic deposits

Terrigenous deposits include marlstone and siliciclastic lithofacies, alternating with travertine in the studied succession but also forming the substrate alternating with volcanic and volcanoclastic deposits. They are generally intercalated with travertine deposits possessing a reduced metre-scale thickness, while in the northern part of the study area, a mixed carbonate siliciclastic upper Pleistocene-Holocene thick succession (about 25 m thick) occurs at the top of travertine deposits.

#### *Palaeosoil*

This lithofacies (Figure 4a1,a2,a3,a4) is characterized by a maximum thickness of 1.5 m, with tabular and concave-upward lenticular geometries generally characterized by basal erosional surfaces. The lithofacies laterally passes into intraclast lithofacies, while it unconformably overlies all the different travertine deposits. In the study area, palaeosoil generally shows brown-orange colours with associated karst features such as cavities with variable dimensions filled by carbonate mud, clay, travertine intraclasts, speleothems and vadose pisoids and rare terrestrial vertebrate bones. Collapsed breccias comprising metre and decametre fragments from overlying layers with heterogeneous grain size are common and well developed in the central and southern part of the study area. The presence of silt, clay and angular travertine intraclasts suggests periods of subaerial exposure that could be also related to ephemeral fluctuations of the water table (Faccenna et al., 2008).

#### *Claystone and Marlstone deposits*

This lithofacies (Figure 4b1,b2,b3) is characterized by variable thickness and lateral extension. In core C5, it reaches 5 m in thickness, while a maximum value of 2 m was measured in outcrop. The geometry is mostly tabular, passing laterally into all the travertine lithofacies described. This lithofacies type (F1 black to dark grey mudstone, F5 white to light brown marl and F6 green to brown fine sand, silt and clay in Della Porta, Croci, et al., 2017) is mainly composed of fine-grained silt, sand and clay. The colour varies between dark brown and yellow. Fragments of plants as well as cm–mm intraclasts frequently occur, locally organized in about

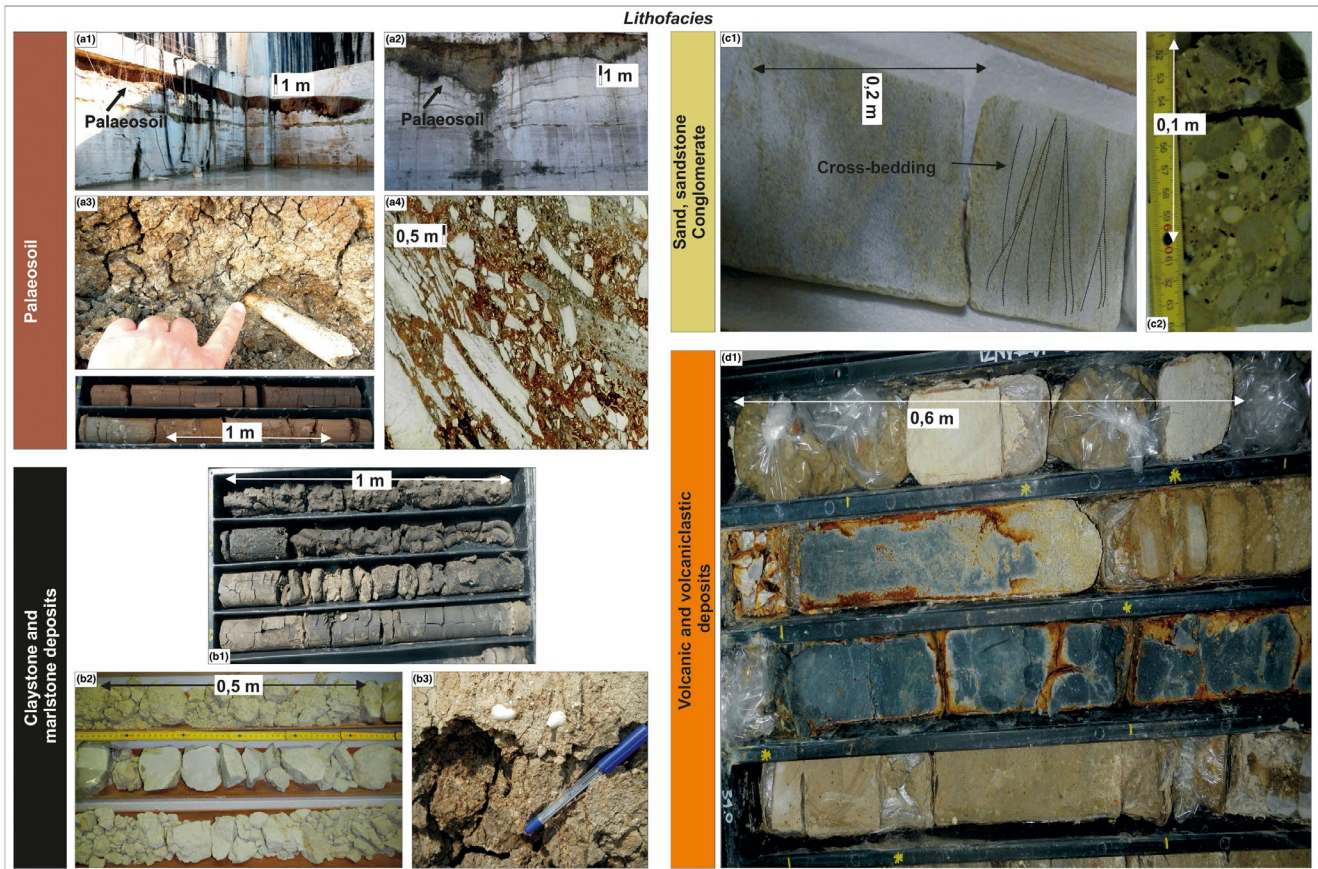


**FIGURE 4** Terrigenous deposits. (a1, a2, a3, a4) Palaeosol lithofacies. (b1, b2, b3) Claystone and marlstone deposit lithofacies. (c1, c2) Sand, sandstone and conglomerate lithofacies. (d1) Volcanic and volcanoclastic deposits

20 cm lenses or as sparse material in the matrix. These fine-grained deposits, sometimes rich in organic matter, testify for stagnant, or poorly oxygenated freshwater conditions. Ponds, wetland marshes, shallow lacustrine to palustrine settings represent the environments where these deposits developed.

#### *Sand, sandstones and conglomerate*

These lithofacies (F7, F9 and F10 in Della Porta, Croci, et al., 2017) principally occur in the southern part of the study area and are observed in some boreholes, where they reach a maximum thickness of 4 m (core C8 and C9). Polymictic, well-sorted conglomerate (Figure 4c1,c2), locally with fine sandy matrix and occasionally with ‘flame structures’ and sandstone with cross-bedding and cross-lamination are the most common features associated with these deposits, displaying lenticular geometries. Conglomerates include extraclasts (0.5–1 cm in diameter) from the Meso-Cenozoic limestone cropping out in the surrounding Apennine Mountains. According to Della Porta, Croci, et al. (2017), these deposits were related to fluvial channels of the Aniene River.

#### *Volcanic and volcanoclastic deposits*

Deposits related to the activity of different volcanic complexes present in the area (Colli Albani and Sabatini; Della

Porta, Croci, et al., 2017), generally showing different colours from brown, black, grey and red (Figure 4d1). Sometimes these deposits are altered by pedogenic processes leading to the formation of soils with predominant brown colours. The volcanic pyroclastic deposits and volcanic ashes (F2, F3, F4 in Della Porta, Croci, et al., 2017) show a maximum thickness of 5 m and display mostly tabular geometries. They crop out in the northern and southern part of the basin (Colle Fiorito and Aniene River; see Figure 1c).

## 4.2 | Depositional system

The sedimentary succession filling the Acque Albule Basin is characterized by lithofacies developed in a continental setting. The lithofacies underlying the *Lapis Tiburtinus* travertine are characterized by claystone and marlstone in the northern part, palaeosol interfingering with claystone and marlstone in the central part and fluvial deposits in the southern part of the study area. These types of deposits can be related to an alluvial plain depositional environment passing towards the southern part of the study area to a fluvial depositional environment (cf. Della Porta, Croci, et al., 2017).

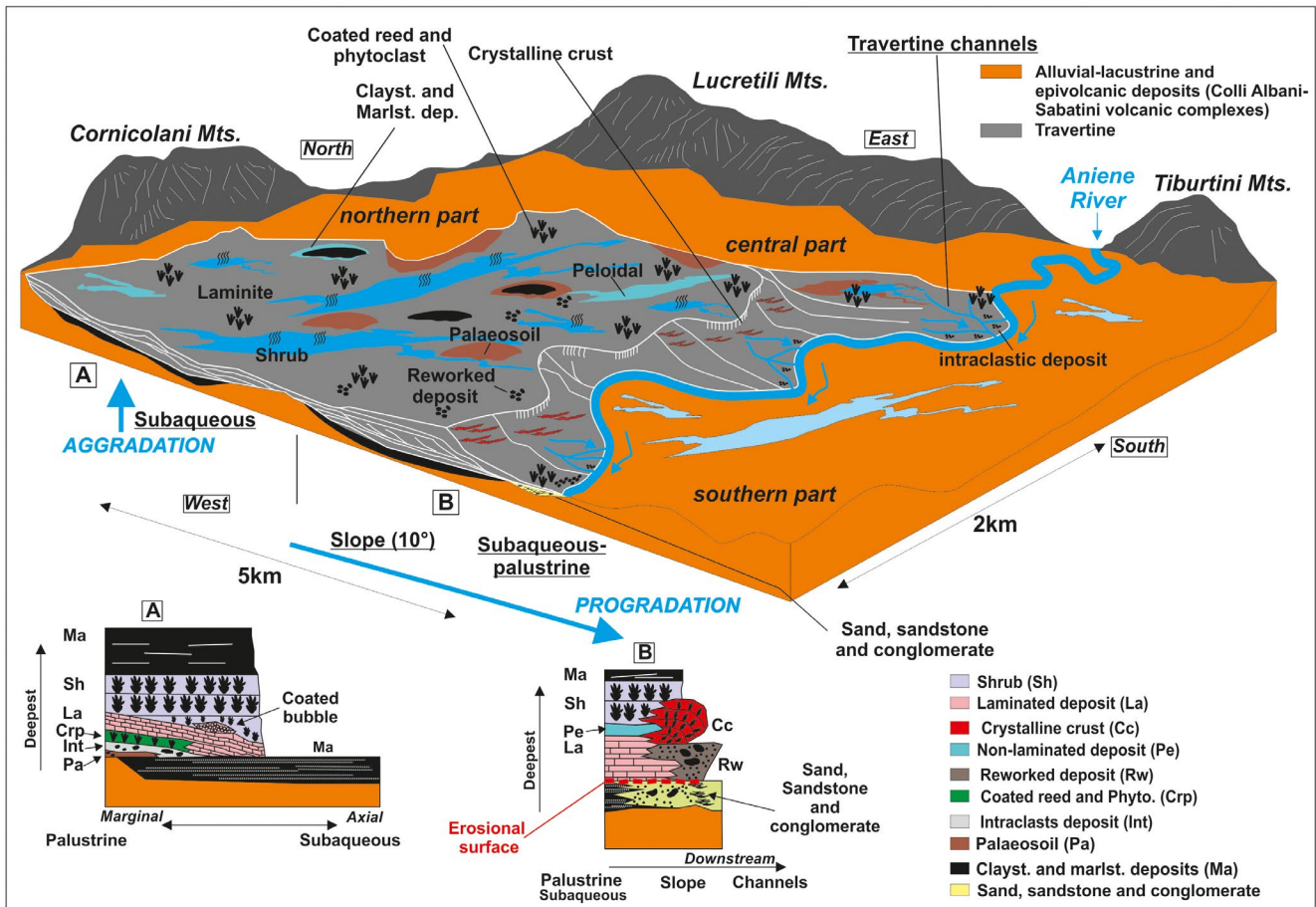


**FIGURE 5** Depositional model of the *Lapis Tiburtinus* travertine and lithofacies association distribution showing the aggradational–progradational patterns in the northern, central and southern part of the basin. (A, B.) Synthetic stratigraphic logs representative of the northern and central-southern parts of the study area

Only in the borehole-core C4, the travertine deposits directly overlie the volcanic and volcanoclastic deposits, otherwise alluvial plain and lacustrine deposits are comprised between the volcanic and the travertine deposits (cf. Della Porta, Croci, et al., 2017).

Lithofacies associations observed in different parts of the study area allow identifying four main depositional environments: subaqueous, palustrine, travertine channel and slope (Figure 5).

The subaqueous environment is typically characterized by alternation (or predominance) of lithofacies associations related to shrub, laminated deposit displaying aggradational patterns laterally passing to claystone and marlstone deposits. In fact, the shrub and laminated deposit lithofacies associations typically develop in low-energy depositional conditions such as shallow lakes, waterlogged flats and pools, and only locally are associated with inclined surfaces. This is observed in the northern part of the study area, while the claystone and marlstone lithofacies, sometimes rich in organic matter, testify for stagnant, or

poorly oxygenated freshwater conditions (ponds, wetland marshes, shallow lacustrine settings).

The palustrine environment is formed by the association of non-laminated deposit, laminated deposit and coated reed and phytoclast lithofacies, alternating with intraclast deposit and palaeosol. Generally, these lithofacies associations show an aggradational trend. The palustrine environment occurs in the marginal portion of shallow lakes and toe of slope, characterized by stagnant water settings with well-developed vegetation. This environment was affected by fluctuations related to climatic oscillations associated with alternation of humid and arid conditions or seasonal changes. The non-laminated lithofacies type develops in stagnant pool environments or in shallow flat ponds, with terrigenous and freshwater input, testified by the presence of ostracods and *Charophytes* (Della Porta, Croci, et al., 2017). The coated reed and phytoclast lithofacies is typical of flat marshes with occasional subaerial exposure testified by palaeosol. The abundant presence of plants indicates environmental conditions suitable for their development, suggesting the influence of distal cooled

thermal water or/and mixed with freshwater (Della Porta, Croci, et al., 2017).

The travertine channel environment is characterized by the presence of reworked deposit, related to travertine erosion and high-energy depositional conditions. The presence of well-rounded clasts, the imbrication and the bed load traction structures suggest the influence of a fluvial setting on travertine depositional system. As also reported by Özkul et al. (2013) and Brogi et al. (2010), erosion and breakage of travertine carbonates produce lithoclasts transported downstream by the river and accumulated in depressions and ponds located in distal areas (Guo & Riding, 1998; Jones & Renault, 1995). Generally, the orientation of the travertine channels is N-S, in the direction of the southern Aniene River.

The slope environment is typically represented by crystalline crust associated with laminated deposit and occasionally coated reed and phytoclast lithofacies. Such lithofacies association resembles high-energy setting with very thin sheets of water flowing over a planar, low-angle slope surface (7°–10°) and rapid CO<sub>2</sub> degassing (Della Porta, Croci, et al., 2017; Guo & Riding, 1998). This lithofacies association is typically present in the central and the southern part of the area, with a progradational trend and a drainage system directed towards the southern part or locally towards the E or W.

The *Lapis Tiburtinus* travertine displays aggradational and progradational stacking patterns. Aggradational patterns, typical of the northern part, are the most common and originate from very shallow, gently inclined and sub-horizontal areas (subaqueous environment) where travertine lithofacies developed. Progradational patterns are particularly pronounced in the lateral, marginal parts (palustrine environment) and in the central-southern portion (towards the Aniene River) where relatively steep angle slope deposits accumulated. Downlap geometries between different travertine units are locally present on the frontal (southern) portion of the sloping surfaces. These stratal patterns, together with N–S-oriented travertine channel system, corroborate the interpretation of flowing water towards the Aniene River, inducing the system to prograde towards the south.

### 4.3 | Bounding surfaces and sedimentary units: Geobody architecture of the *Lapis Tiburtinus* travertine

The Acque Albule Basin covers an area of 28 km<sup>2</sup> with a travertine volume of 1.1 km<sup>3</sup>. The extraction activity and the many related quarries present in the study area offer the possibility to develop 3D imaging of most of the basin sedimentary filling.

Different unconformity surfaces due to non-deposition and erosion (labelled as V, B1–B9) can be correlated in the study area, bounding 10 depositional units (labelled as

U1–U10) that make up the geobody architecture of the *Lapis Tiburtinus* travertine (Figure 6). The lowermost surface (V in this study; S5 sensu Faccenna et al., 2008) represents the boundary between the travertine deposits and the underlying terrigenous and volcanic and volcanoclastic deposits.

This surface overlies the Pleistocene volcanic deposits derived from the Colli Albani and Sabatini volcanic complexes, intercalated with claystone, silt and marlstone from lacustrine and alluvial plain deposits and fluvial sand, sandstone and conglomerate (cf. Della Porta, Croci, et al., 2017). Fluvial channel intercalations are observable only in the southern part of the study area (C8 and C9 cores).

In the northern part, bounding surfaces are generally covered by intraclast lithofacies or thin layers of brown claystone and marlstone deposits. In the central part, these surfaces mainly show erosional bases. Locally, they are overlain by palaeosol and claystone and marlstone deposits filling small depressions possibly formed during periods of subaerial exposure (e.g. in quarries F and G). In the southern part of the study area, unconformity surfaces are laterally discontinuous and lenticular, in general associated with grey-brown claystone and marlstone and reworked lithofacies.

The topographic surface (T), with a mean elevation of 60 m a.s.l., is locally characterized by karstic phenomena, expressed by the presence of metre and decametre-scale sinkholes affecting travertine deposits (Billi et al., 2016; Salvati & Sasowsky, 2002).

The different bounding unconformity surfaces are reported in Table 3. In Table 4, the 10 resulting geobodies (U1–U10) are individually detailed based on their lithofacies composition (the correlation panel is reported in Figure S2).

The travertine depositional units reconstructed (Figures 7–9) are described below starting from base to top and are compared with the previous subdivision and age dating performed by Faccenna et al. (2008), Erthal et al. (2017) and Della Porta, Croci, et al. (2017).

- *U1* (115–99 ka; Unit B4 sensu Faccenna et al., 2008; U1 sensu Della Porta, Croci, et al., 2017). This unit represents the first depositional event only observable in the studied deep boreholes. The total volume of this unit is 0.16 km<sup>3</sup> with a thickness of 17 m in the northern part, 15 m in the central part and 5 m in the southern part of the study area. Lenticular concave-upward geometries in the northern, central and southern parts with aggradational pattern in the whole area and a progradational pattern towards the SE and NE part of the study area characterize the entire unit U1, which is not laterally continuous. In the northern part, this unit is mainly composed of centimetre layers of intraclast deposit (C4 core) alternating with laminated deposit, while in the western part of the study area (C5 core), pyrite-rich claystone layers vertically pass to non-laminated lithofacies. In the central part instead, U1 is only composed of

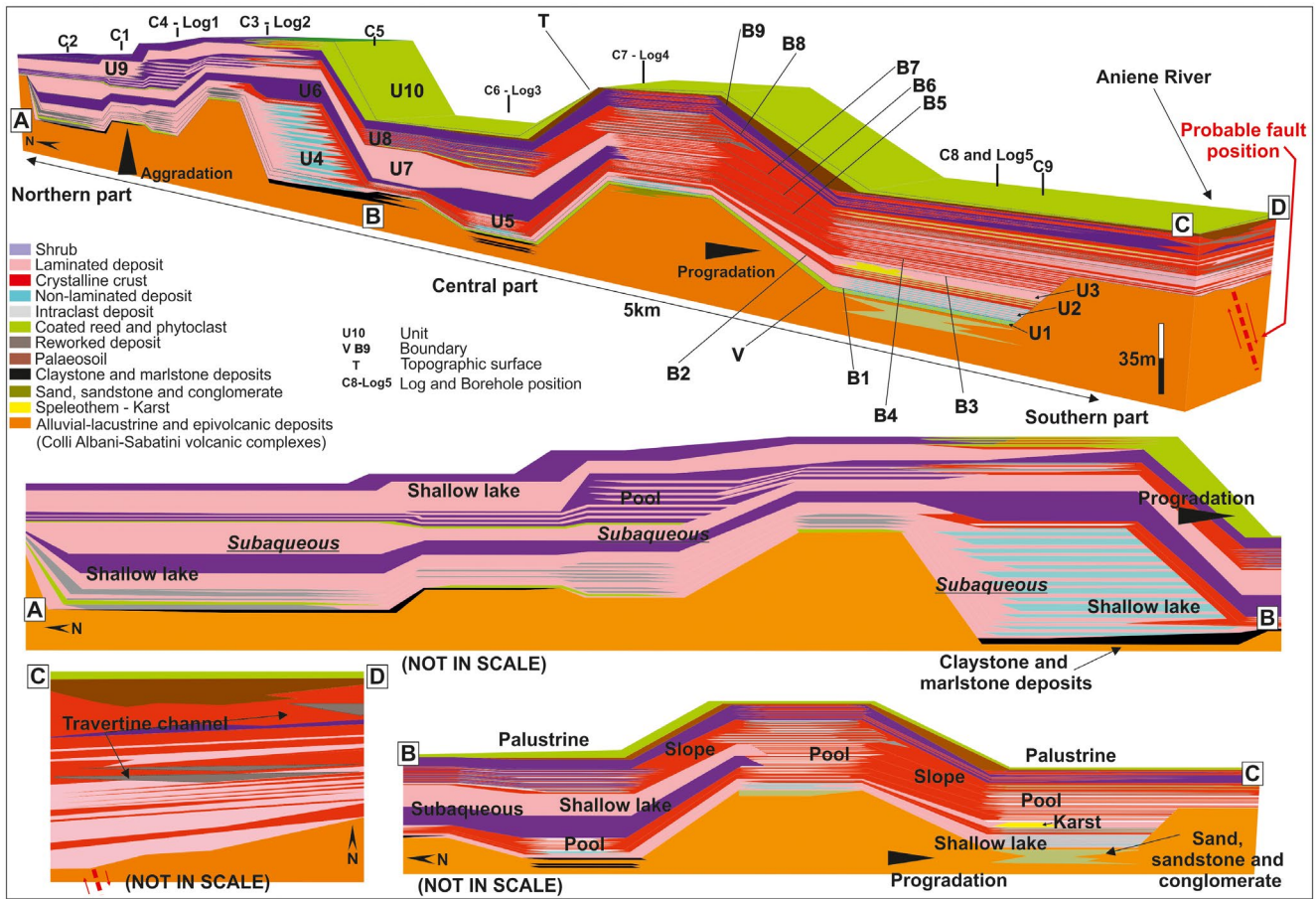


**FIGURE 6** 3D model of the studied travertine succession. The *Lapis Tiburtinus* travertine is divided into ten different units that are characterized by different lithofacies associations. The study area is distinguished in a northern, central and southern part. The northern and central parts are both characterized by thick (40–70 m) travertine deposits. The southern part is instead characterized by a thin (35 m) succession of travertine. In the northern part, it is possible to observe the predominance of subaqueous deposits, with tabular and concave-upward geometries related to shallow lake and pool deposits, based on the lithofacies association. A slope environment characterizes the central part passing laterally to a subaqueous environment towards the southern and northern part of the study area. Lenticular convex-upward geometries characterize the central part, while concave-upward geometries, principally related to pools and shallow lakes, are locally present in this part of the study area. Travertine channel deposits pass laterally to slope deposits and are visible in the central and southern part of the study area. In general, they are associated with lenticular shapes with a progradational pattern towards the S

marlstone and claystone deposits (C2, C3 and C6 core). The southern part is characterized by the presence of non-laminated deposit. The lithofacies association attests for a deposition in pools or shallow lakes affected by freshwater input (C2, C3 and C6 core) typical of low-energy palustrine-subaqueous settings, locally affected by anoxic conditions (distal zone sensu Capezzuoli et al., 2014).

- U2 (99–82 ka: Unit B4 sensu Faccenna et al., 2008; U2 sensu Della Porta, Croci, et al., 2017). Similarly, to U1, also this unit is modelled only from data acquired from the studied borehole cores. The total volume is 0.04 km<sup>3</sup> with a thickness of 3 m in the northern part, 6 m in the central part and 2 m in the southern part of the study area. Unit U2 is laterally discontinuous and characterized by tabular geometries in the northern part and lenticular concave-upward geometries in the southern and central parts of the study area. A progradational trend

towards the NE part of the study area characterizes this unit in the northern and central part, while aggradational and progradational patterns towards the SE are observed in the southern part. Alternation of coated reed and phytoclast lithofacies with intraclast and laminated lithofacies occurs in the northern and western part of the study area, while in the central-southern part, non-laminated deposit is vertically alternating with laminated lithofacies (C8–C7 cores). Coated reed and phytoclast lithofacies is generally only observable in the southern part. The presence of this lithofacies in the northern part (core C3) could be correlated with a more humid period, or with the presence of another spring located in the North of the study area. In fact, this unit and its lithofacies association testify for a generally low-energy depositional environment that can be separated in a subaqueous setting in the northern part and palustrine in

**TABLE 3** Description of the bounding unconformity surfaces in the northern, central and southern part of the study area

Surface	Boundary between	Northern part	Central part	Southern part
B1	U10–U9	Erosive surface covered by recent clastic deposits	Erosive surface covered by recent clastic deposits (locally sinkholes)	Discontinuity with associated palaeosoils
B2	U9–U8	Discontinuity covered by claystone	Discontinuity covered by claystone	Discontinuity, locally erosive with associated palaeosoils
B3	U8–U7	Discontinuity covered by claystone	Discontinuity covered by claystone	Discontinuity covered by claystone
B4	U7–U6	Discontinuity covered by claystone and breccia deposits	Erosive surface with depressions filled by intraclast deposits and locally claystone	Discontinuity covered by claystone
B5	U6–U5	Discontinuity covered by claystone and breccia deposits	Erosive surface with depressions covered by palaeosoils and breccia deposits	Discontinuity covered by claystone, locally associated with karst
B6	U5–U4	Discontinuity covered by claystone and breccia deposits	Erosive surface with depressions filled by intraclast deposits	Discontinuity covered by claystone and breccia deposits
B7	U4–U3	Discontinuity covered by claystone and breccia deposits	Discontinuity covered by claystone, breccia deposits and marlstone	Erosive surface with depression filled by reworked deposits
B8	U3–U2	Discontinuity covered by claystone and breccia deposits	Erosive surface with associated depressions covered by breccia deposits, palaeosoils and claystone	Erosive surface covered by palaeosoils and claystone
B9	U2–U1	Discontinuity	Discontinuity	Discontinuity covered by clastic deposits
V	Travertine – Terrigenous and volcanic deposits	Discontinuity	Discontinuity covered by volcanic deposits	Discontinuity covered by sandstones and conglomerates

the central-southern part, with freshwater input (distal zone sensu Capezzuoli et al., 2014).

- *U3* (99–82 ka; Unit B4 sensu Faccenna et al., 2008; U3 sensu Della Porta, Croci, et al., 2017). This unit, exposed in the central-southern quarries (F, H, L quarries and C9 borehole), was modelled using both field and borehole data. The total volume of this unit is 0.08 km<sup>3</sup> with a thickness of 3 m in the northern part, 5 m in the central part and 2 m in the southern part of the study area. This unit, which is laterally discontinuous, is characterized by lenticular convex-upward geometries in the northern part with progradational pattern towards the NE part and tabular to lenticular concave-upward geometries in the southern part with progradational pattern towards the S. In the central part instead, U3 shows aggradational features together with progradation towards the South. Laminated deposit associated with shrub lithofacies association characterizes unit U3 in the northern part (C4 core). In the central-western part, instead, an association of laminated and non-laminated lithofacies is predominant (C5 core). Karstification processes and speleothems are recognizable (C9 core) in the southern part of the study area (cf. Della Porta, Croci, et al., 2017). The lithofacies association is indicative of a subaqueous depositional

environment in the northern and central parts of the study area (distal zone sensu Capezzuoli et al., 2014) and a slope environment in the western part, oriented towards the southern part of the study area (intermediate-distal zone sensu Capezzuoli et al., 2014).

- *U4* (99–82 ka Unit B4 sensu Faccenna et al., 2008; U4 sensu Della Porta, Croci, et al., 2017). This unit crops out in the lower middle part of the quarry walls within the southern (M, L quarries) and central part (F quarry) of the study area. The total volume of this unit is 0.03 km<sup>3</sup> with a thickness of 4 m in the northern part, 6 m in the central part and 3 m in the southern part of the study area. This unit, which is laterally discontinuous, is characterized by lenticular convex-upward geometries in the northern part with progradational pattern towards the NE part of the study area, while in the central part, lenticular concave-upward geometries identify the unit. Tabular geometries with progradational trend towards the axis of the study area define the unit in the southern part. Laminated deposit represents the main lithofacies of unit U4, sometimes interbedded with intraclast lithofacies (B, C, D and F quarries, C6 core). In the southern part of the study area (lower part of L quarry), this unit is characterized by alternating laminated and crystalline



**TABLE 4** Description of depositional units with the lithofacies associations in the northern, central and southern part of the study area, with geometries and thickness (for more details see text). ‘Testina’ is the local name used to identify a poorly lithified travertine, corresponding with U10

Unit	Northern part lithofacies	Central part lithofacies	Southern part lithofacies	Geobody Geometries	Thickness (m)
U10 – ‘Testina’	Shrub	Crystalline crust	Crystalline crusts	Tabular	10 – 3
		Coated reed and phytoclast	Coated reed and phytoclast	Lenticular convex-upward Lenticular concave-upward	
U9	Laminated deposit	Shrub	Crystalline crust	Tabular	5 – 2
			Shrub	Lenticular convex-upward Lenticular concave-upward	
U8	Laminated deposit	Laminated deposit	Crystalline crust	Lenticular convex-upward	4 – 3
	Shrub	Shrub	Reworked deposit	Lenticular concave-upward Tabular	
U7	Shrub	Shrub	Laminated deposit	Lenticular convex-upward	7 – 2
			Crystalline crust	Lenticular concave-upward Tabular	
U6	Shrub	Shrub	Laminated deposit	Lenticular convex-upward	9 – 4
			Crystalline crust	Lenticular concave-upward Tabular	
U5	Shrub	Laminated deposit	Laminated deposit	Tabular	5 – 3
		Crystalline crust	Crystalline crust	Lenticular convex-upward Lenticular concave-upward	
U4	Laminated deposit	Laminated deposit	Laminated deposit	Lenticular convex-upward	6 – 3
	Intraclast deposit	Non-laminated deposit	Crystalline crust	Lenticular concave-upward	
U3	Laminated deposit	Laminated deposit	Non-laminated deposit	Lenticular convex-upward	5 – 2
	Intraclast deposit	Non-laminated deposit	Speleothem	Lenticular concave-upward Tabular	
U2	Intraclast deposit	Non-laminated deposit	Non-laminated deposit	Lenticular concave-upward	6 – 2
	Laminite	Laminated deposit	Laminated deposit	Tabular	
U1	Intraclast deposit	Marlstone and Claystone	Non-laminated deposit	Lenticular concave-upward	17 – 5
	Laminite			Tabular	

crust lithofacies, with the latter decreasing in the south-western portion of the study area (quarry M). The depositional environments vary from subaqueous in the central and northern part to high energy steeply dipping settings in the southern part. The central-southern part of the study area is characterized by laminated deposit and crystalline crust lithofacies attesting for a high-energy and turbulent slope environment (intermediate-distal zone sensu Capezzuoli et al., 2014). A local palustrine environment (distal zone sensu Capezzuoli et al., 2014) characterizes the SE and E parts of the study area.

- U5 (99–82 ka; Unit B4 sensu Faccenna et al., 2008; U5 sensu Della Porta, Croci, et al., 2017). This unit crops out in the E, L, B, C and D quarries. The total volume of this unit is 0.04 km<sup>3</sup> with a thickness of 3 m in the northern part, 5 m in the central part and 3 m in the southern part of the study area. This unit, which is laterally continuous, has lenticular convex-upward

geometries with progradational pattern towards the NW part and tabular to lenticular concave-upward geometries with progradational pattern towards the S part, in the northern and central-southern portion, respectively. In the northern part, shrub lithofacies is predominant (B, C and D quarries), while laminated deposit and crystalline crust lithofacies characterize the unit in the other part of the study area. The entire unit reflects deposition in subaqueous conditions.

- U6 (99–82 ka; Unit B4 sensu Faccenna et al., 2008; part of U6 sensu Della Porta, Croci, et al., 2017; subsequence 1.1 sensu Erthal et al., 2017). This unit represents the top of the quarries in the southern part of the study area (L quarry and C9 borehole), while in the northern-central part, it is observable in the upper portion of the B, C, D, E, F and G quarries. The total volume of this unit is 0.12 km<sup>3</sup> with a thickness of 4 m in the northern part, 9 m in the central part and 5 m in the southern

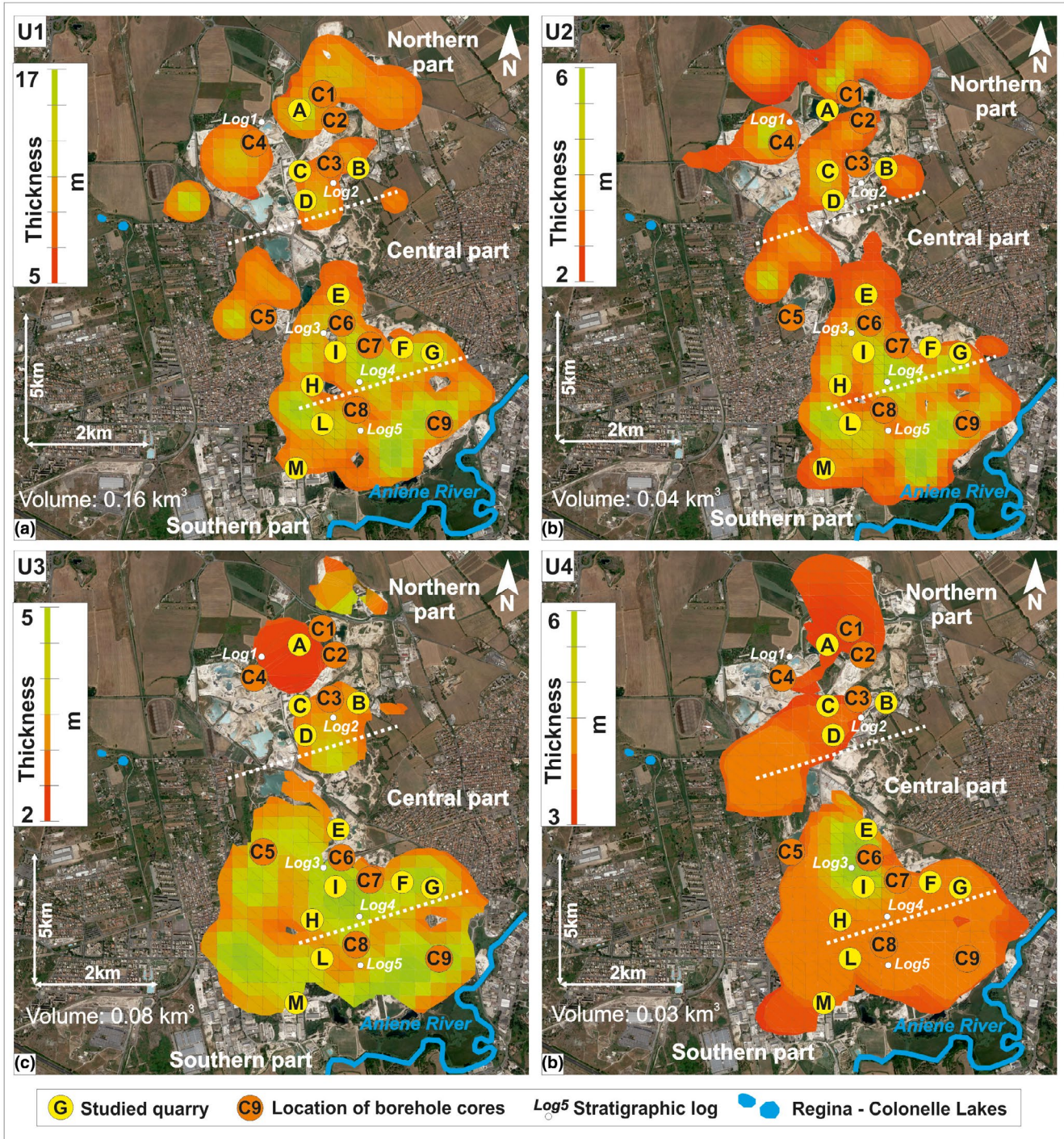


**FIGURE 7** Reconstructed units U1 (a), U2 (b), U3 (c) and U4 (d). The different colours indicate the thickness. Volume values are also indicated for every unit

part of the study area. U6 is laterally continuous throughout the entire study area. Lenticular convex-upward geometry characterizes the unit in the northern part, with progradational pattern towards the NE and NW. Lenticular concave-upward geometries with progradational pattern towards the S part are instead typical of the central part of the study area, while tabular geometries characterize the southern part, with a progradational pattern towards the S. Laminated deposits interbedded with

crystalline crust lithofacies are observable in the central and southern parts (C5 core), while in the northern part, centimetre-thick layers of shrub lithofacies association (C1 and C2 cores) characterize the unit. The lithofacies association is representative of different environmental settings reflecting subaqueous conditions in the northern part, slope environment with a low angle (10°; Della Porta, Croci, et al., 2017; Erthal et al., 2017) (intermediate-distal zone sensu Capezuoli et al., 2014) in the

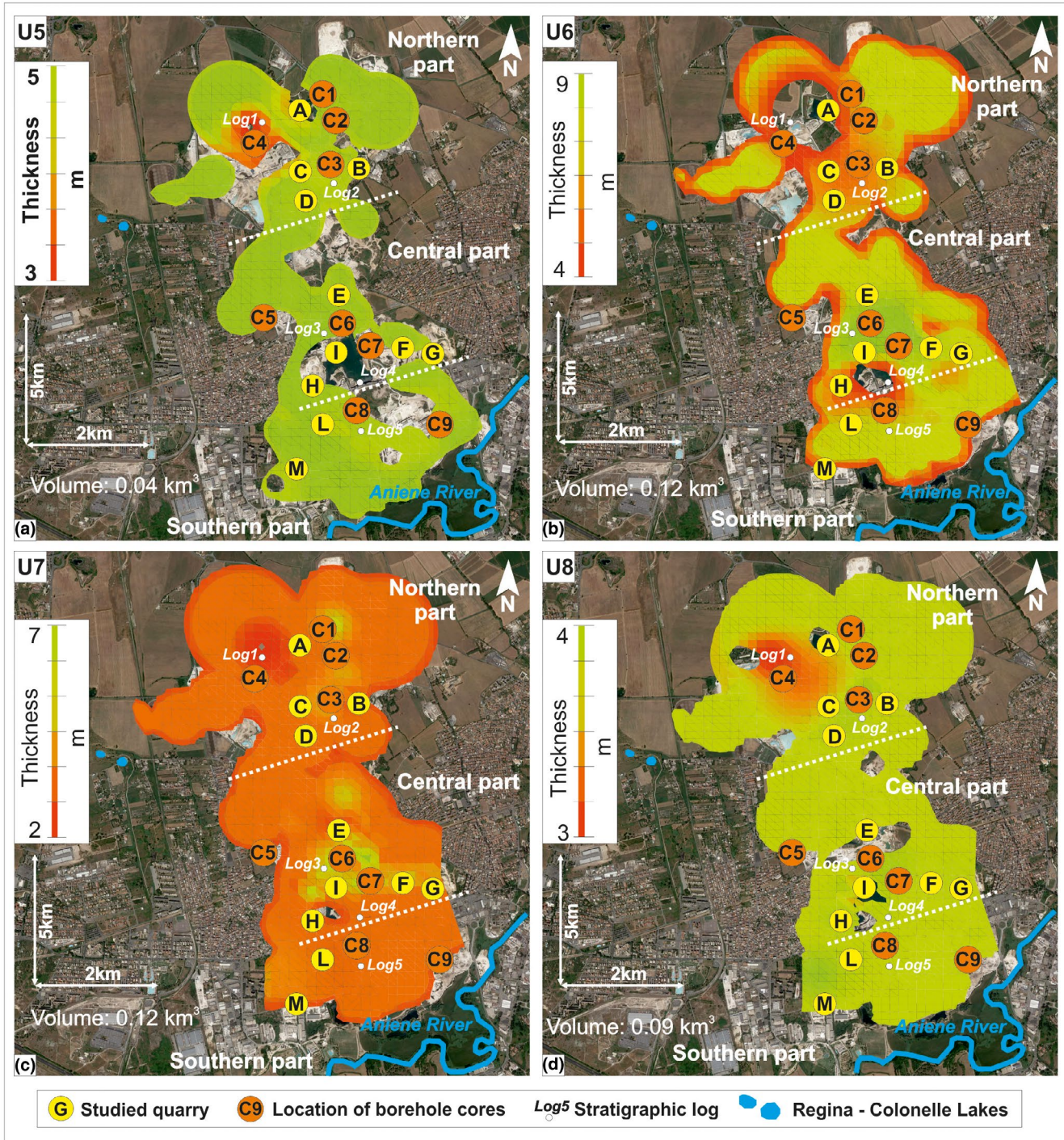


**FIGURE 8** Reconstructed units U5 (a), U6 (b), U7 (c) and U8 (d). The different colours indicate the thickness. Volume values are also indicated for every unit

central part and subaqueous conditions in the southern part (distal zone sensu Capezzuoli et al., 2014).

- U7 (82–56.5 ka; Unit B4 sensu Faccenna et al., 2008; part of U7 sensu Della Porta, Croci, et al., 2017; subsequence 1.2 sensu Erthal et al., 2017). This unit is observable in all quarries within the study area. The total volume of this unit is 0.12 km<sup>3</sup> with a thickness of 7 m in the northern part, 5 m in the central part and 2 m in the southern part. This unit is laterally

continuous. Tabular and lenticular convex-upward geometries with a progradational pattern and increasing thickness towards the eastern part of the study area characterize the unit in the northern part. The central-southern part is instead defined by tabular geometries with progradational pattern towards the S. Shrub lithofacies association is predominant over the entire unit. Only in the central part of the study area (B, C and D quarries), centimetre-thick shrub layers are interbedded with

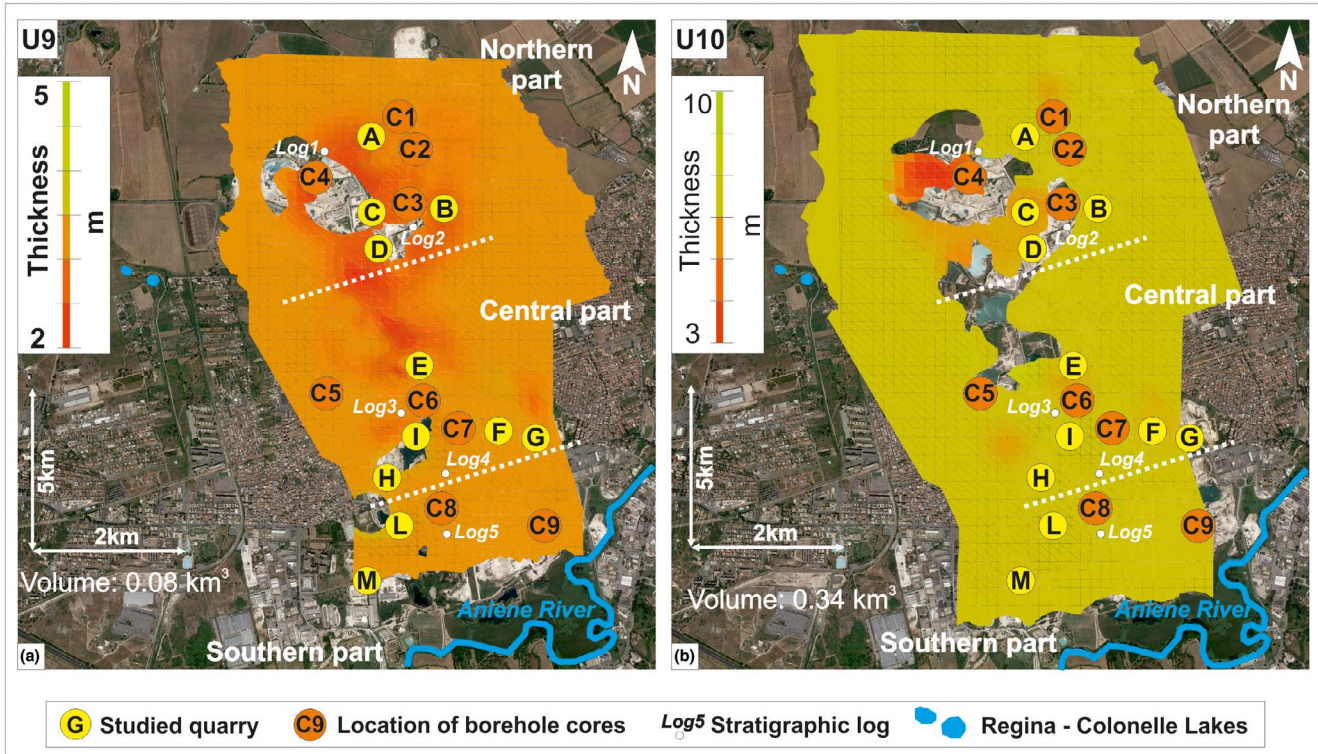


**FIGURE 9** Reconstructed U9 (a) and U10 (b). The different colours indicate the thickness of the units. Volume values are also indicated for every unit

laminated lithofacies, while towards the W (C1 and C2 cores) laminated deposit and shrub layers are interbedded with crystalline crust lithofacies, attesting for subaqueous depositional environments (intermediate-distal zone sensu Capezzuoli et al., 2014).

- U8 (82–56.5 ka; Unit B3 sensu Faccenna et al., 2008; part of U8 sensu Della Porta, Croci, et al., 2017; sequence 2 sensu Erthal et al., 2017). This unit, well exposed in quarries M and A, with a total volume of 0.09 km<sup>3</sup>, has a thickness of 3 m in the northern part, 4 m in the central part and 3 m in the southern part of the study area. The unit, which is laterally continuous, is characterized by lenticular convex-upward geometries with a progradational pattern with an angle of about 10° from the western part (quarry A) towards the eastern part (C1 and C2 cores). The central part is also characterized by tabular geometries with progradational pattern towards the SW. Lenticular concave-upward geometries associated with reworked deposits with progradational pattern toward the SW part of the study area characterize unit U8 in the southern part. The dominant lithofacies association is constituted by the laminated deposit, especially in its northern portion, while shrubs are locally present towards the NW (quarry A). The depositional environment is generally subaqueous.
- U9 (56.5–44 ka; Unit B2 sensu Faccenna et al., 2008; part of U9 sensu Della Porta, Croci, et al., 2017; sequence 3.1 and 3.2 sensu Erthal et al., 2017). This unit is observable in all quarries of the study area. The total volume of this unit is 0.08 km<sup>3</sup> with

a thickness of 2 m in the northern part, 5 m in the central part and 2 m in the southern part of the study area. Unit U9, which is laterally continuous, shows lenticular convex-upward and concave-upward geometries in the northern and in central part of the study area with progradational pattern towards the NE and the SE parts, respectively. Instead, tabular geometries with a progradational pattern towards the S are present in the southern part. Lithofacies related to this unit are variable, with laminated lithofacies, predominant in B, C and D quarries (detailed in Erthal et al., 2017) as well as the in the C1 and C2 cores. Nonetheless, in the north-eastern part of the study area, shrub lithofacies is interbedded with laminated lithofacies (quarry A), while in the southern part, crystalline crust lithofacies becomes progressively dominant. In correspondence with C5 core, unit U9 is characterized by the presence of intensive dark to brown colour marlstone and claystone deposits. The depositional environments are variable with subaqueous settings in the central and northern parts of the study area, while slope and travertine channel environments characterize the southern part (intermediate-distal zone sensu Capezzuoli et al., 2014).

- U10 (44–30 ka; Unit B1 sensu Faccenna et al., 2008). The uppermost unit of the *Lapis Tiburtinus* travertine is traditionally known as ‘Testina’ (Faccenna et al., 2008) and crops out in all visited quarries. The total volume of this unit is 0.34 km<sup>3</sup> with a thickness of 4 m in the northern part, 10 m in the central part and 3 m in the southern part of the study area. This unit is laterally continuous in the whole area with different geometries. In

the northern part, the geometries are lenticular convex-upward (quarry A), while in the eastern part, it is lenticular concave-upward (C1 and C2 cores) with progradational pattern towards the NE part of the study area. In the central and southern parts, the geometry is dominantly tabular with a progradational pattern towards the S. Rapid lateral lithofacies changes characterize the entire unit with shrub lithofacies in the northern part (quarries A, B, C and D), crystalline crust and coated reed and phytoclast lithofacies in the central part (quarries E, F and H) and southern part (quarry M). Regarding the depositional environment, unit U10 lithofacies reflects subaqueous conditions in the northern and central parts, with evidence of slope environments in the central-southern part (intermediate zone sensu Capezzuoli et al., 2014). Palustrine environments become predominant in the southern part of the study area, close to the Aniene River (distal zone sensu Capezzuoli et al., 2014).

## 5 | DISCUSSION

### 5.1 | Processes affecting the geometry and architecture of travertine deposits

Alternating humid and dry climatic or seasonal phases directly control the water availability in an aquifer, with humid periods characterized by the predominance of vegetation and related biogenic lithofacies, as for example, the coated reed and phytoclast lithofacies observed in the *Lapis Tiburtinus* travertine, and dry periods, in general associated with subaerial exposure and erosion (Claes et al., 2015; De Filippis, Anzalone, et al., 2013; De Filippis, Faccenna, et al., 2013; Della Porta, Capezzuoli, et al., 2017; Della Porta, Croci, et al., 2017; Guo & Riding, 1998). The location of the active springs instead is related to fault position and activity while local topography, hydrology, water flow type and composition, and carbonate precipitation rate control the travertine geometries, characterized by tabular bodies, mounds and aprons with steep slopes (Della Porta, Capezzuoli, et al., 2017; Della Porta, Croci, et al., 2017).

Claes et al. (2015) focused on travertine deposits of the Denizli Basin (Turkey). These travertine deposits are 70 m thick and cover an area of 1,800 m in width and 5,000 m in length. The travertine succession was divided into dominantly subaqueous deposits, characterized by sub-horizontal travertine facies, formed in depressions affected by physical erosion during drops or even periodic interruption of carbonate precipitation due to discontinuous water flow or changes in flow path. The subaerial (thin water film) deposits, instead, were related to slope settings, with precipitation taking place on a topographic relief due to higher precipitation rate, close to the springs with decreasing water calcium carbonate supersaturation along the flow path. The boundary

between these two systems is marked by the deposition of the marl-conglomerate facies, which reflects a lacustrine system, temporarily interrupted and cut by rivers. According to Van Noten et al. (2013), the spring locations in the Denizli Basin were controlled by tectonic activity, with a travertine depositional system affected only by evaporation and degassing processes (Claes et al., 2015).

Della Porta, Capezzuoli, et al. (2017), addressing the few square kilometre wide travertine succession of Acquasanta Terme (Central Italy), recognized two travertine aprons consisting of four aggradational-progradational units, which were separated by erosional unconformities produced by events of non-deposition and erosion, due to temporary interruptions of vent activity, shifts of the vent location and/or deviation of the flow directions. Also in this case, travertine geometries were linked to local topographic gradients, location and morphology of the hydrothermal vents, rates and chemistry of thermal water discharge, influenced by the substrate rocks as well as tectonic and climatic regime (Janssens et al., 2020).

Guo and Riding (1998), studying Rapolano Terme travertine (Central Italy), proposed that calcium carbonate precipitation was rapid and variable, affecting the lateral and vertical facies changes. Switches of vent location, fluctuations in water flow volume and direction, thermal water mixing with cool rainwater, climatic effects and subaerial reworking and pedogenic processes were the most important factors controlling the evolution of the travertine sequence. The combined effects of these factors allowed identifying the travertine geobody architecture (Guo & Riding, 1998).

The *Lapis Tiburtinus* travertine evolution was, according to Faccenna et al. (2008), mostly controlled by water table fluctuations and partly modulated by climatic oscillations, fault-related deformation and volcanic activity. Deposition occurred during the high stands of the water table, whereas erosion occurred under subaerial conditions during water table low stands. Based on U-Th dating performed on the *Lapis Tiburtinus* travertine, Faccenna et al. (2008) suggested that climatic controls affected the evolution of this deposit. In fact, travertine deposition started during the Marine Isotopic Stage MIS 5E, characterized by warm humid conditions (Emiliani, 1955; Shackleton, 1969). This condition, according to Faccenna et al. (2008), enhanced travertine precipitation, but cannot be the only cause for the onset of travertine deposition. The end of the *Lapis Tiburtinus* deposition (30 ka) coincided with the onset of cold and dry periods of the isotopic stage MIS 2 (Emiliani, 1955; Shackleton, 1969), which probably caused a lowering of the water table hampering fluid circulation (Faccenna et al., 2008).

Faccenna et al. (2008) hypothesized that fault-related deformation mainly controls water flowing from the springs, affecting the depositional rate and the travertine formation.

De Filippis, Anzalone, et al. (2013) and De Filippis, Faccenna, et al. (2013), comparing the *Lapis Tiburtinus*

travertine with the travertine deposits cropping out in the Denizli Basin (western Turkey), reported that these two case studies are influenced by palaeoclimate oscillations at regional and global scales as also reported by Hancock et al. (1999) and Uysal et al. (2009). According to De Filippis, Anzalone, et al. (2013) and De Filippis, Faccenna, et al. (2013), in both examples, travertine growth preferentially occurred when the water table was high (warm and/or humid periods), whereas when the water table was depressed (cold and/or dry periods), the *Lapis Tiburtinus* travertine deposits were affected by erosional processes. Palaeoclimatic oscillations appear to control the amount of fluids discharged and the architecture of the deposits.

Anzalone et al. (2017) suggested that the environments where the *Lapis Tiburtinus* travertine develops are related to gentle slope to shallow lake settings. Furthermore, the higher frequency millennial-scale cyclicity recorded in the borehole core studied is attributed to climatic changes influencing water table fluctuations.

## 5.2 | Processes affecting travertine deposits in the Acque Albule Basin

Understanding the predominant factors controlling geobodies architecture in travertine deposits remains a challenging task, especially for the *Lapis Tiburtinus* travertine, for reasons of its several kilometre scale. However, the

study area (10 km<sup>2</sup>) permits some considerations. As part of the Roman Basin, the Acque Albule Basin developed from the Gelasian (early Pleistocene), with a stratigraphic framework strictly influenced by the interaction between tectonic uplift, volcanic activity (Milli et al., 2016 and references therein) and eustatic oscillations. This basin is crossed by the Tiber River as the main collector and its related tributaries, among which the Aniene River is the most important one. Milli et al. (2016) provided a depositional model of the internal (fluvial portion) and external (coastal and marine portion) parts of the Tiber River valley, suggesting that the entire fluvial depositional system, and also the related tributary network, responded to relative sea-level falls and rises and to related changes in sediment supply. The Tiber River was strictly influenced by glacio-eustatic sea-level changes and by concomitant volcanism and tectonics (Giustini et al., 2020; Milli, 1997; Milli et al., 2008) controlling the position and the orientation of the Tiber-incised valley and delta mouth, as well as the tributary rivers flowing into the Tiber River (e.g. the Aniene River; Milli et al., 2016). The Tiber River depositional system was divided into two depositional sequences: the Monte Mario and Ponte Galeria sequences (respectively MMS and PGS sensu Milli et al., 2016; their figure 8.19). According to Milli et al. (2016), the PGS sequence and its subdivisions (PG1–PG9) are characterized by fluvial, fluvio-palustrine-lacustrine deposits, interfingering with volcanic deposits of

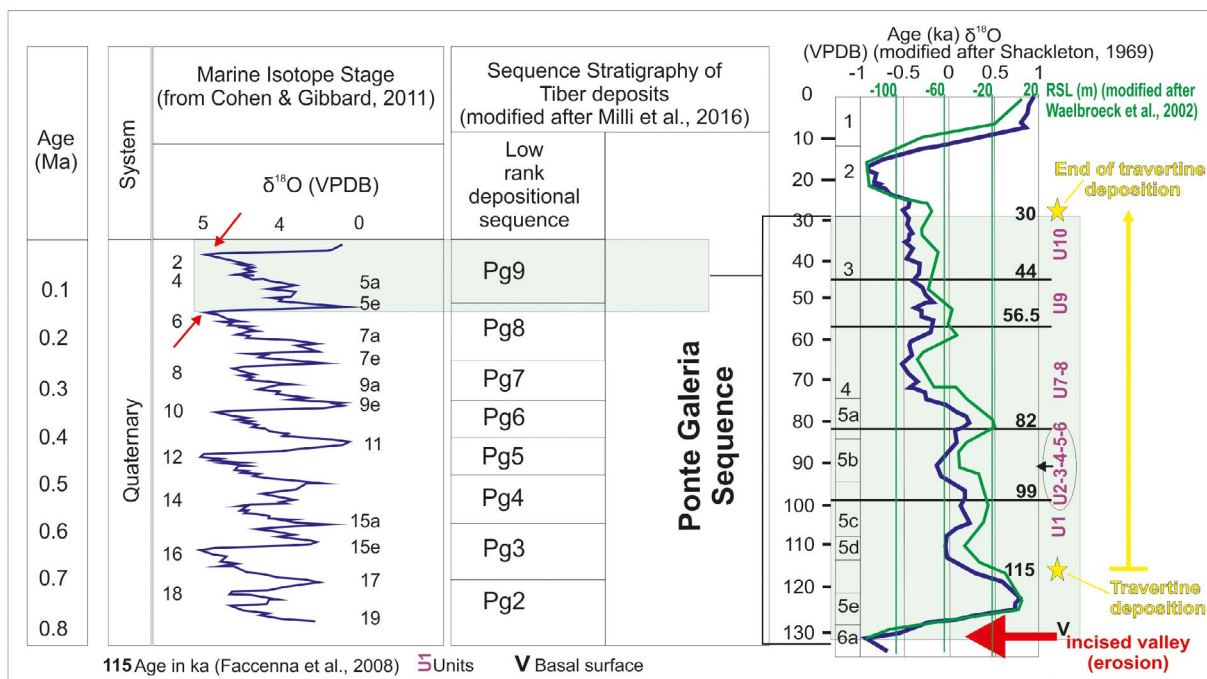


**FIGURE 10** Marine isotope stages and glacio-eustasy compared with the stratigraphy of the Tiber River deposits (Roman Basin). The time interval of PG9 (Milli et al., 2016) is coeval with the deposition of the *Lapis Tiburtinus* travertine in the Acque Albule Basin. The radiometric ages obtained by Faccenna et al. (2008) are reported as well as the temporal distribution of the units detailed in this study and the relative sea-level fluctuations (modified after Cohen & Gibbard, 2011; Milli et al., 2016; Shackleton, 1969; Waelbroeck et al., 2002)

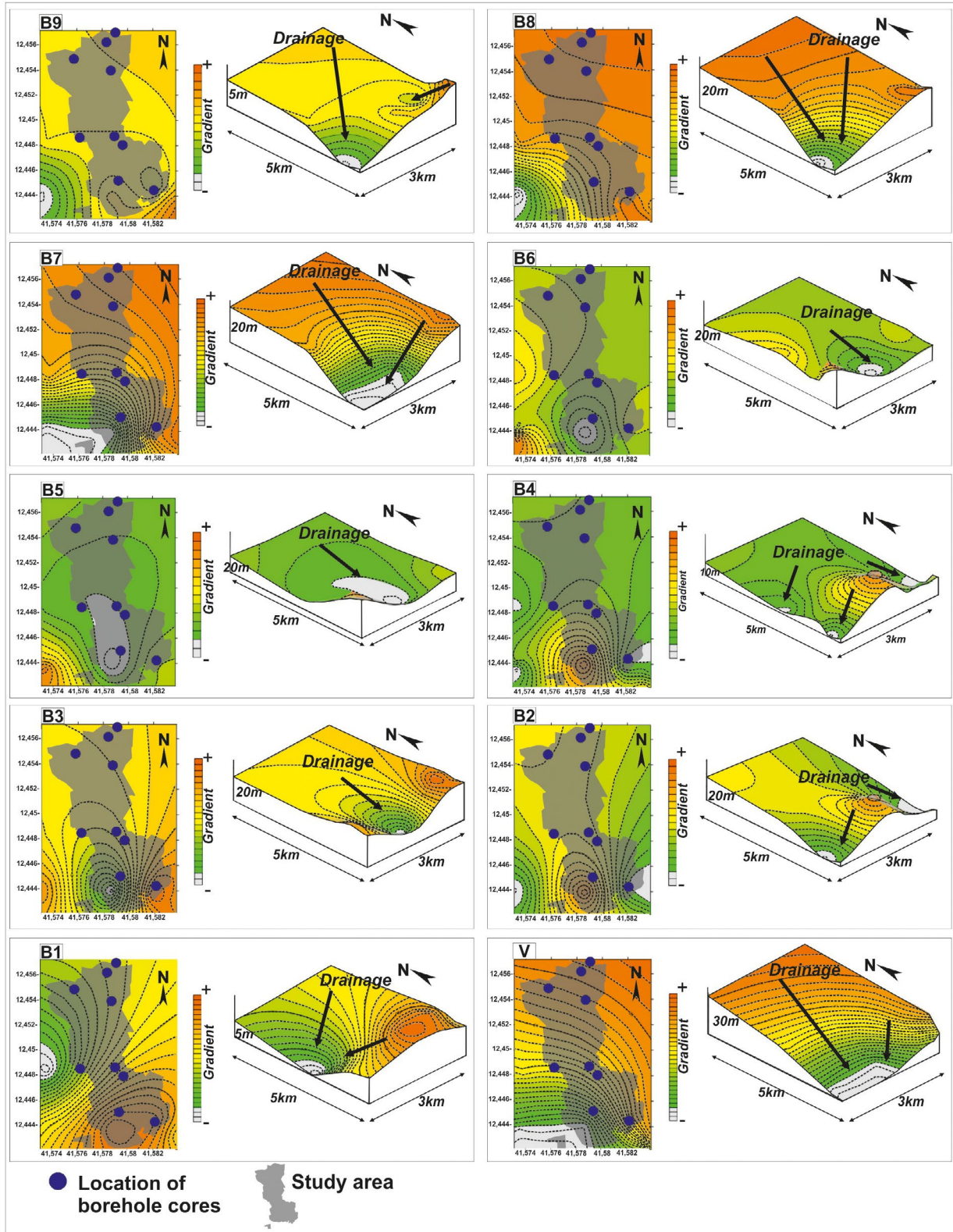


**FIGURE 11** Diagrams representing the different surfaces bounding the *Lapis Tiburtinus* travertine geobodies. Their reconstruction and shape highlight the presence of depressions with lenticular concave-upward shape filled by travertine deposits. The presence of these elongated, N–S-oriented depressions could be explained as travertine channel systems with drainage flows towards the southern part of the basin to the Aniene River

the Albani and Sabatini volcanic complexes. Such depositional organization is similar to the deposits described in cores C5, C8 and C9 (Della Porta, Croci, et al., 2017) below the V surface. According to Faccenna et al. (2008), the deposition of travertine started at  $115 \pm 12$  ka continuing till  $29 \pm 4$  ka. Hence, PG9 can be considered coeval

with the *Lapis Tiburtinus* travertine and its basal surface (V) can be correlated with the eustatic sea-level fall of MIS 6. Interestingly, also the reported end of the travertine deposition coincides with a eustatic fall (MIS 2), also related to a glacial period (Last Glacial Maximum – LGM; Clark et al., 2009; Faccenna et al., 2008) (Figure 10).

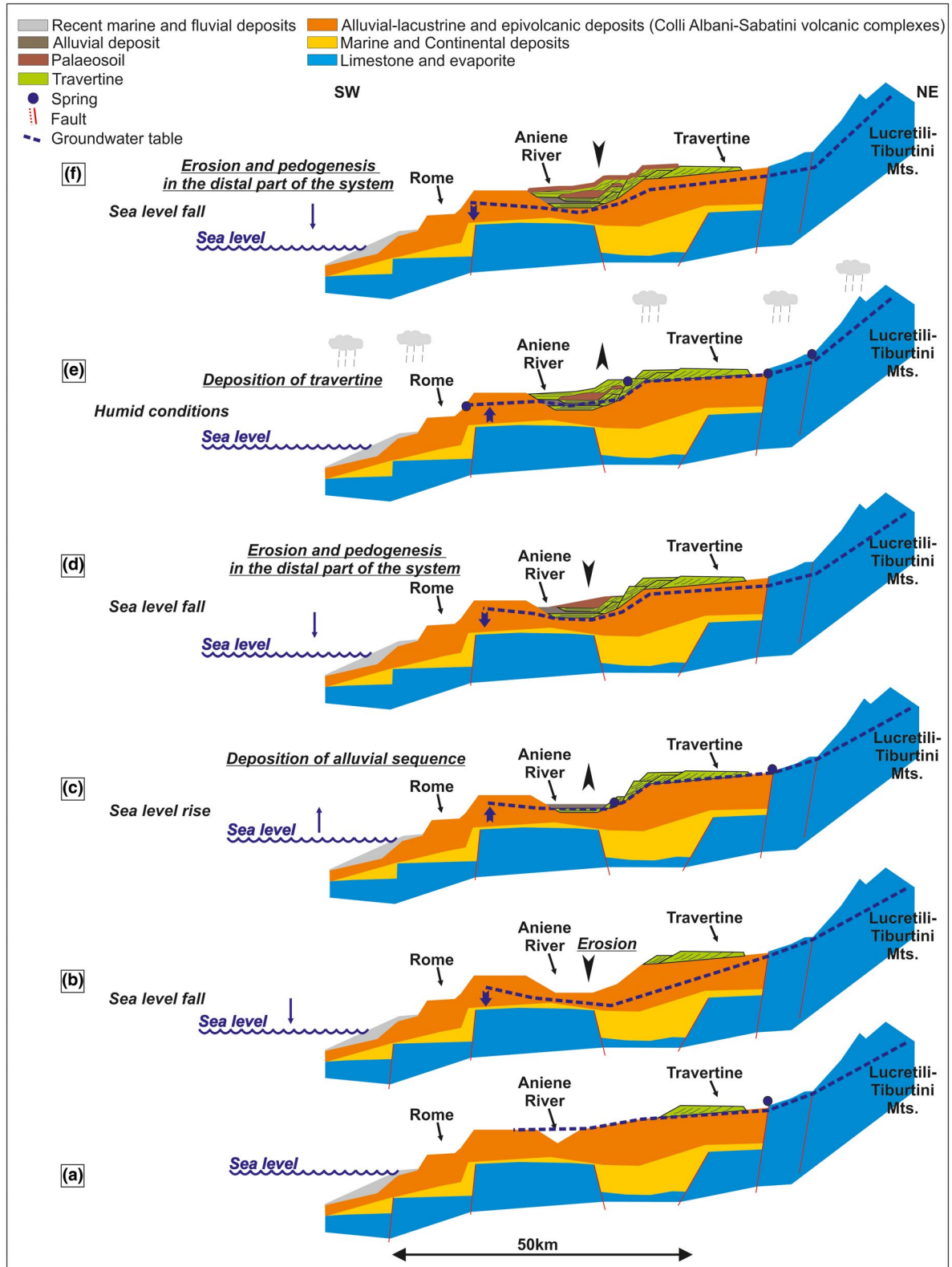




**FIGURE 12** Depositional model showing the evolution of the sedimentary fill of the Acque Albule Basin and the deposition of the *Lapis Tiburtinus* travertine in relation to eustatic sea-level fluctuations. Stage A: initial stage showing the travertine depositional system and the Aniene River fluvial valley. Stage B: the sea-level fall produces erosion and incision of the fluvial valley by the Aniene River. Stage C: the sea-level rise produces the upward migration of the groundwater table and the activation of the springs in different sectors of the study area. Discharge rate from the springs of water supersaturated with respect to calcium carbonate increases. In this Stage C, travertine deposits show progradational trend filling the space produced by the erosion developed during Stage B, associated with alluvial depositional sequences. Stage D: the sea-level fall produces the migration downwards of the groundwater table and the decrease of spring activity with associated erosion and pedogenesis in the distal part of the travertine depositional system. Stage E: humid conditions associated with increased rainfall produce the upward migration of the groundwater table and the re-activation of the springs with deposition of travertine, without any fluctuation in sea level. Stage F: the sea-level fall produces the erosion and pedogenesis in the distal part of the travertine depositional system, associated with the migration downwards of the groundwater table. The fall in sea level associated with cold arid climate during glacial phases produces the lowering of the groundwater table and the erosion of the travertine deposits, as well as the development of palaeosols (Stages B, D and F). The rise in sea level and the increased rainfall during warm humid interglacial phases induce the upward migration of the groundwater table and the activation of the springs at different elevations (Stages C and E). In this scenario, tectonic activity only controls the permeability and the circulation of the hydrothermal fluids and eustatic oscillations control the space used for accumulating travertine deposits (modified after Carucci et al., 2012; Giustini et al., 2020)

The travertine channel environment, described in this study (Figures 2, 5 and 6) for the first time in the area of the Acque Albule Basin, is characterized by high-energy conditions. Such type of environment developed in the central and southern parts of the study area (Figure 2). Özkul et al. (2013) described similar depositional environments in travertine deposits from Turkey, with similar sedimentological features, but their evolution is related to local factors such as the degradation and erosion of travertine due to intense rainfall. The travertine channel environment of the *Lapis Tiburtinus* travertine is instead well developed within the entire travertine succession, interconnecting the lenticular depressions, and filled by the travertine deposits. Also the surfaces bounding the units are generally associated with reworked and intra-clast lithofacies (central-southern part of the basin) with erosional features, locally possessing lenticular concave-upward geometries. The 3D model of such surfaces and the oriented cross-sections highlight the lenticular shapes, as well as their lateral migration with a progradational pattern of travertine units towards the southern part of the basin (see Figure 6).

Eustatic sea-level falls can cause incision, even affecting areas far away from the coastline (up to 1,000 km; Boyd et al., 2006). Similarly to other travertine examples (see Janssens et al., 2020), it is evident how relative sea-level falls and rises controlled river base-level oscillations and the evolution of the related travertine system. In the Acque Albule Basin, the Aniene River affected the evolution of the travertine channel environments recognized in the *Lapis Tiburtinus* travertine and the interconnection between the different depressions where travertine accumulated. Such hypothesis is supported by the fact that the N–S orientation of the channels remains constant in the entire travertine succession and is independent from the progradation–aggradation pattern of the travertine units (Figure 11).

### 5.3 | Climate changes and tectonic activity

Tectonic activity of an N-S striking, right-lateral seismically active fault (Gasparini et al., 2002) (Figure 12) controls the location and distribution of active thermal springs, sink-holes and other karstic features (Billi et al., 2016; Faccenna et al., 2008; Minissale et al., 2002; Pentecost & Tortora, 1989; Salvati & Sasowsky, 2002). Evidence of faulted or displaced travertine in the Acque Albule Basin is reported by Faccenna et al. (2008) and hypothesized by De Filippis, Faccenna, et al. (2013) and Anzalone et al. (2017) in the northern part of the basin. Conversely, clear evidences of faults in the central and in the southern part of the studied area are absent. The different geobodies possess undisturbed high lateral continuity (more than 400 m; Erthal et al., 2017) which is only locally disturbed by fractures (De Filippis, Faccenna, et al., 2013) (Figure 13a–c).

However, faults may have developed in other geographic positions within the Acque Albule Basin, enhancing rock permeability, hydrothermal circulation and the sites of the active springs. De Filippis, Faccenna, et al. (2013) suggested that water discharged at the springs can be considered one of the most important factors controlling the rise of thermal water as well as the opening of fractured conduits feeding the travertine deposits. Based on this hypothesis, De Filippis, Faccenna, et al. (2013) suggested that high pressure of thermal water produces the opening of conduits as well as the subsidence of the Acque Albule Basin, creating a shallow lake environment fed by hydrothermal conduits and subsiding during the last 100,000 years with a subsidence rate of 0.4 mm/yr. These geothermal springs issue water rich in  $\text{CaCO}_3$  favouring the precipitation also far away from the spring location. Because travertine deposits cover the most important faults developed in the

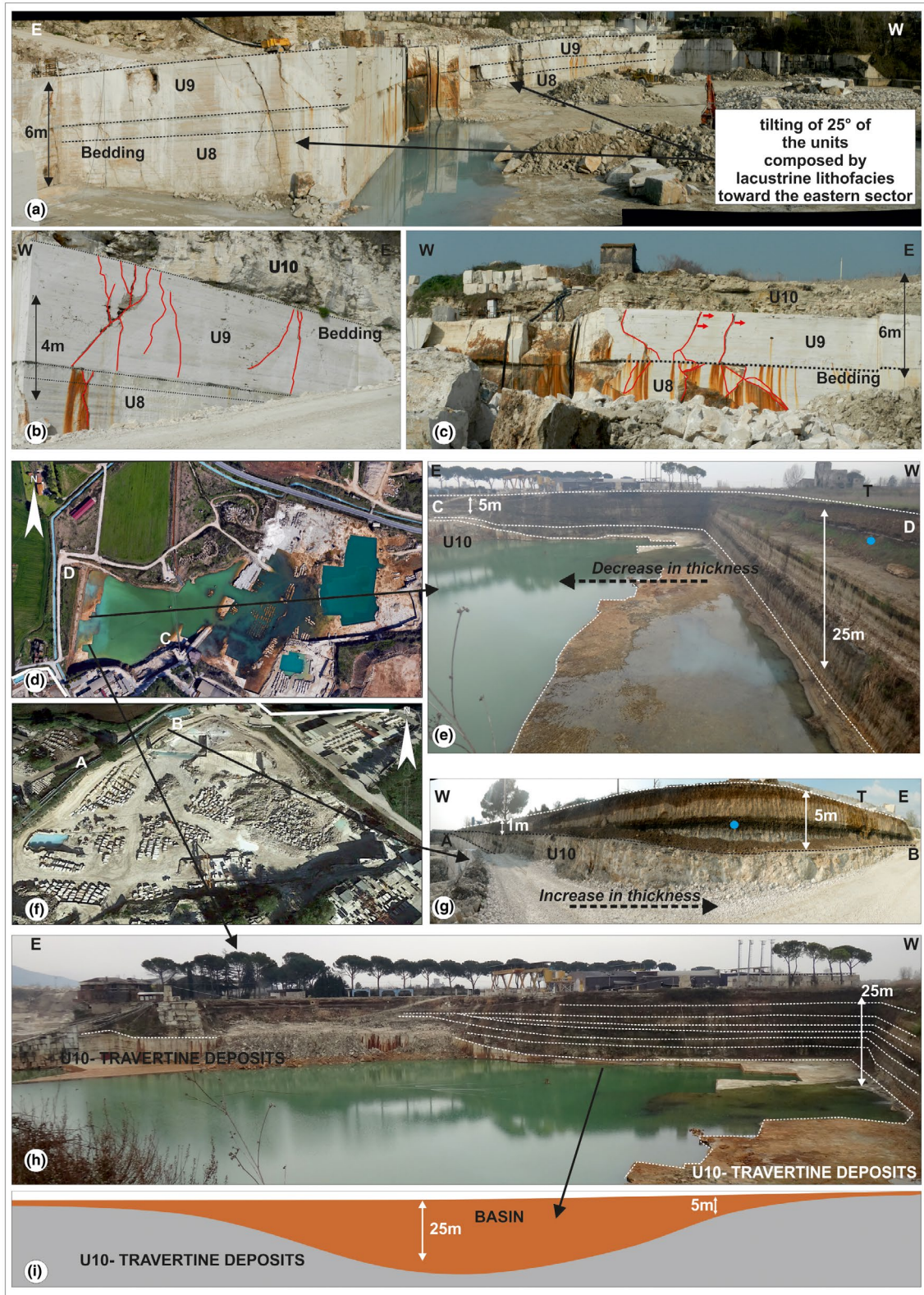


**FIGURE 13** (a–c) Fractures affecting the travertine deposits in the northern part of the study area and tilting of the travertine deposits of  $25^\circ$  towards the NE part of the study area. (d–f) Quarries in the northern part of the study area characterized by mixed carbonate-siliciclastic deposits on top of the travertine succession. As shown in images e and g, the thickness of the succession increases towards the eastern sector of the study area (the blue dot indicates the same stratigraphic position of a claystone layer). (h, i) Lenticular geometry with concave-upward basal surface associated with the mixed carbonate-siliciclastic deposits on top of travertine succession, interpreted as sub-kilometre size basin (panoramic views of the quarries are modified from Google Earth; Digital Globe, 2018)

Acque Albule Basin, these faults are only observable in the north, affecting the Jurassic-Miocene marine carbonate succession cropping out in the Cornicolani Mountains. In this area, deformation associated with these faults produces N-S striking, right lateral faults and N30°–40°-striking, transtensional-to-normal faults as well as a N40°-striking set of joints affecting also the Plio-Pleistocene deposits and the Pleistocene volcanic deposits of the area (Faccenna et al., 2008).

This set of joints is observable also in the northern part of the study area (Figure 13d–f), where a NE-tilted (about 25°) travertine succession (U8, U9 and U10) is present (Figure 13a–c). This is conformably overlain by a clastic sequence with an evident lenticular concave-upward geometry (Figure 13e,g–i) (up to 25 m in its thickest portion). Such tilting and the lateral change are, according to Faccenna et al. (2008), related to fault activity but could also be explained as local subsidence (Billi et al., 2016; Salvati & Sasowsky, 2002).

Palaeoclimate and water table fluctuations instead exerted a major control on the travertine lithofacies associations (cf. De Filippis, Anzalone, et al., 2013; De Filippis, Faccenna, et al., 2013). Faccenna et al. (2008) suggested that the evolution of the Acque Albule Basin and its sedimentary filling is characterized by stages of deposition and erosion. These stages are associated with palaeoclimatic cycles (i.e. cold-to-warm and humid-to-dry oscillations) that controlled the fluctuations of the groundwater level.

Based on the data presented in this study, the Acque Albule Basin can be considered as a system of flat incised-valleys that were fluvially eroded by the Aniene River, with a low elongated topography. The relationships between glacio-eustatic sea-level fluctuations, tectonic and volcanic activity are predominant factors leading and controlling the architecture of the Acque Albule Basin. The possibility to recognize the influence of eustatic and base-level oscillations in a travertine depositional system permits to evaluate better the evolution of the depositional units at basin scale. The Pleistocene Acque Albule Basin is located less than 45 km far away from the Tyrrhenian Sea. The results of this study suggest that the *Lapis Tiburtinus* travertine accumulated in a depositional system characterized by kilometre-size sub-basins, associated with subaqueous conditions. Such sub-basins were interconnected with each other by a well-developed hydrographic travertine channels network, characterized by higher energy conditions, evolved and controlled through time by the Aniene River base-level fluctuations.

The former fluctuations seem able to highly influence the evolution of the travertine architecture in the Acque Albule Basin over short periods of time (100,000 year), while tectonic features probably were able to condition travertine evolution at a longer time scale (500,000 year).

## 5.4 | Travertine versus carbonate platform

This study provides additional data supporting a similarity between travertine depositional systems and marine carbonate platform with respect to the control exerted by accommodation and sea-level fluctuations on the architecture of sedimentary units. D'Argenio et al. (2008) reported about the similarity of travertine deposits with marine carbonates platforms. The flat-topped geometry passing laterally into a steeper slope resembles the profile of a high-relief carbonate platform and the aggradational and progradational depositional trends modulated by the upward and downward shifts in elevation of the active springs mimic the effects of relative sea-level changes in marine carbonate platforms (Della Porta, Capezzuoli, et al., 2017; Della Porta, Croci, et al., 2017). Moreover, Martín-Algarra et al. (2003) described a perched spring tufa system highlighting that the geometry and growth style of these freshwater carbonates with pools, dams and cascades resemble marine reef terraces of prograding carbonate platforms. Until now, travertine depositional systems have been considered outside the influence of eustatic fluctuations, but this study suggests how this factor can play an important role in the evolution and in the stacking pattern of travertine units at basin scale, highlighting also in this case the possible similarity with marine carbonate platforms.

## 6 | CONCLUSIONS

The performed 3D model highlights the importance of combining different approaches to identify geobodies, surface geometries and their spatial distribution at basin scale in continental settings. This study, supported by quantitative data collected over the entire study area, suggests that the *Lapis Tiburtinus* travertine accumulated in a kilometre-size sub-basinal setting with subaqueous conditions interconnected by a hydrographic channel network evolved and controlled through time by the fluctuation of the Aniene River base level. Tectonic activity is considered important at the sedimentary basin scale and over a long (hundreds of thousands to million years) time frame with regard to the evolution of the Acque Albule Basin, influencing the basinal subsidence through time and the location of the active springs. However, climatic changes influence the rainfall precipitation rate and the groundwater level, and not the distribution and the geometries of the sub-basins at basin scale. Such sub-basins, expanding and merging in a unique final depositional setting, developed mainly under the control of Aniene River base level linked to glacio-eustatic fluctuations.

## ACKNOWLEDGEMENTS

A special thank go to Shell, Total and Petrobras to support the TraRas project and to the quarry owners (Alessandro,

Francesco, Maurizio, Francesca, Aurelio and Roberto of Querciolaie-Rinascente and Pacifici quarries), who granted the possibility to access the quarries and for the logistic supports. The borehole cores investigated by Giovanna Della Porta and integrated in the data set here presented were donated by Equinor ASA to Giovanna Della Porta and the University of Milan. H. Nijs is acknowledged for the preparation of thin sections. Many thanks to Tonino and to Franco and Figli restaurant for the logistic support. We are grateful to Editor Wonsuck Kim, M. Cihat Alçiçek and A. Brogi for their useful comments and constructive criticisms that substantially improved the manuscript.

## CONFLICT OF INTEREST

No conflict of interest has been declared by the authors.

## PEER REVIEW

The peer review history for this article is available at <https://publons.com/publon/10.1111/bre.12576>.

## DATA AVAILABILITY STATEMENT

The data that support the findings of this study are available from the corresponding author upon reasonable request.

## ORCID

Alessandro Mancini  <https://orcid.org/0000-0002-2303-6538>

Giovanna Della Porta  <https://orcid.org/0000-0003-3479-0592>

Rudy Swennen  <https://orcid.org/0000-0002-1528-526X>

Enrico Capezzuoli  <https://orcid.org/0000-0002-4199-1870>

## REFERENCES

- Acocella, V., & Funicello, R. (2006). Transverse systems along the extensional Tyrrhenian margin of Central Italy and their influence on volcanism. *Tectonics*, 25, 1–24. <https://doi.org/10.1029/2005TC001845>
- Alçiçek, C. M., Alçiçek, H., Altunel, E., Arenas, C., Bons, P., Brogi, A., Capezzuoli, E., Rised, T., Della Porta, G., Gandin, A., Guo, L., Jones, B., Karabacak, V., Kershaw, S., Liotta, D., Mindszenty, A., Pedley, M., Ronchi, P., Swennen, R., & Temiz, U. (2017). Comment on ‘First records of syn-diagenetic non-tectonic folding in Quaternary thermogene travertines caused by hydrothermal incremental veining’ by Billi et al. *Tectonophysics*, 721, 491–500. <https://doi.org/10.1016/j.tecto.2017.09.002>
- Allen, P. A., & Allen, J. R. (2008). *Basin analysis: Principles and application to petroleum play assessment* (3rd ed.). Wiley-Blackwell. ISBN: 978-0-470-67377-5
- Anzalone, E., D’Argenio, B., & Ferreri, V. (2017). Depositional trends of travertines in the type area of Tivoli (Italy). *Rendiconti Lincei. Scienze Fisiche e Naturali*, 28(2), 341–361. <https://doi.org/10.1007/s12210-017-0595-1>
- Barchi, M. (2010). The Neogene-Quaternary evolution of the Northern Apennines: Crustal structure, style of deformation and seismicity. *Journal of the Virtual Explorer*, 36, 1–24. <https://doi.org/10.3809/jvirtex.2010.00220>
- Bhattacharya, J., & Walker, R. G. (1991). Allostratigraphic subdivision of the Upper Cretaceous Dunvegan, Shaftesbury, and Kaskapau Formations in the subsurface of northwestern Alberta. *Bulletin of Canadian Petroleum Geology*, 39, 145–164.
- Bigi, G., Castellarin, A., Coli, M., Dal Piaz, G. V., Sartori, R., Scandone, P., & Vai, G. B. (1990). *Structural model of Italy 1:50.000, Sheet 1. C.N.R., Progetto Finalizzato Geodinamica*. SELCA.
- Billi, A., De Filippis, L., Poncia, P. P., Sella, P., & Faccenna, C. (2016). Hidden sinkholes and karst cavities in the travertine plateau of a highly-populated geothermal seismic territory (Tivoli, Central Italy). *Geomorphology*, 255, 63–80. <https://doi.org/10.1016/j.geomorph.2015.12.011>
- Billi, A., Tiberti, M. M., Cavinato, G. P., Cosentino, D., Di Luzio, E., Keller, J. V. A., Kluth, C., Orlando, L., Parotto, M., Praturlon, A., Romanelli, M., Storti, F., & Wardell, N. (2006). First results from the CROP-11 deep seismic profile, central Apennines, Italy: Evidence of mid-crustal folding. *Journal of Geological Society London*, 163, 583–586. <https://doi.org/10.1144/0016-764920-002>
- Boyd, R., Dalrymple, R. W., & Zaitlin, B. A. (2006). Estuarine and incised valley facies models. In H. Posamentier & R. G. Walker (Eds.), *Facies Models Revisited* (pp. 171–236). SEPM, Special Publication 84.
- Brogi, A., Capezzuoli, E., Aquè, R., Branca, M., & Voltaggio, M. (2010). Studying travertines for neotectonics investigations: Middle-Late Pleistocene syn-tectonic travertine deposition at Serre di Rapolano (Northern Apennines, Italy). *International Journal of Earth Science*, 99, 1383–1398. <https://doi.org/10.1007/s00531-009-0456-y>
- Brogi, A., Capezzuoli, E., Moretti, M., Olvera-García, E., Matera, P. F., Garduno-Monroy, V. H., & Mancini, A. (2018). Earthquake-triggered soft-sediment deformation structures (seismites) in travertine deposits. *Tectonophysics*, 745, 349–365. <https://doi.org/10.1016/j.tecto.2018.08.021>
- Brunetti, E., Jones, J. P., Petitta, M., & Rudolph, D. L. (2013). Assessing the impact of large-scale dewatering on fault-controlled aquifer systems: A case study in the Acque Albule basin (Tivoli, Central Italy). *Hydrogeology Journal*, 21, 401–423. <https://doi.org/10.1007/s10040-012-0918-3>
- Capelli, G., Cosentino, D., Raffi, R., & Ventura, G. (1987). Modalità di ricarica ed assetto strutturale dell’acquifero delle sorgenti Capore – S. Angelo (Monti Lucretili-Sabina meridionale). *Geologica Romana*, 26, 419–447.
- Capezzuoli, E., Gandin, A., & Pedley, M. (2014). Decoding tufa and travertine (fresh water carbonates) in the sedimentary record: The state of the art. *Sedimentology*, 61, 1–21. <https://doi.org/10.1111/sed.12075>
- Carucci, V., Petitta, M., & Aravena, R. (2012). Interaction between shallow and deep aquifers in the Tivoli Plain (Central Italy) enhanced by groundwater extraction: A multi isotope approach and geochemical modelling. *Applied Geochemistry*, 27, 266–280. <https://doi.org/10.1016/j.apgeochem.2011.11.007>
- Chafetz, H. S., & Folk, R. L. (1984). Travertines: Depositional morphology and the bacterially constructed constituents. *Journal of Sedimentary Research*, 54, 289–316. <https://doi.org/10.1306/212F8404-2B24-11D7-8648000102C1865D>
- Chafetz, H. S., & Guidry, S. A. (1999). Bacterial shrubs, crystal shrubs, and ray-crystal shrubs: Bacterial vs. abiotic precipitation. *Sedimentary Geology*, 126, 57–74. [https://doi.org/10.1016/S0037-0738\(99\)00032-9](https://doi.org/10.1016/S0037-0738(99)00032-9)

- Chafetz, H. S., Rush, P. F., & Utech, N. M. (1991). Microenvironmental controls on mineralogy and habit of CaCO<sub>3</sub> precipitates: An example from an active travertine system. *Sedimentology*, 38, 107–126. <https://doi.org/10.1111/j.1365-3091.1991.tb01857.x>
- Chang, K. H. (1975). Unconformity-bounded stratigraphic units. *Geological Society of America Bulletin*, 86, 1544–1552. [https://doi.org/10.1130/0016-7606\(1975\)86<1544:USU>2.0.CO;2](https://doi.org/10.1130/0016-7606(1975)86<1544:USU>2.0.CO;2)
- Chiodini, G., Cardellini, C., Amato, A., Boschi, E., Caliro, S., Frondini, F., & Ventura, G. (2004). Carbon dioxide Earth degassing and seismogenesis in central and southern Italy. *Geophysical Research Letters*, 31, 1–4. <https://doi.org/10.1029/2004GL019480>
- Claes, H., Soete, J., Van Noten, K., El Desouky, H., Marques Erthal, M., Vanhaecke, F., Özkul, M., & Swennen, R. (2015). Sedimentology, three – dimensional geobody reconstruction and carbon dioxide origin of Pleistocene travertine deposits in the Ballık area (south – west Turkey). *Sedimentology*, 62, 1408–1445. <https://doi.org/10.1111/sed.12188>
- Clark, P. U., Dyke, A. S., Shakun, J. D., Carlson, A. E., Clark, J., Wohlfarth, B., Mitrovica, J. X., Hostetler, S. W., & McCabe, A. M. (2009). The last glacial maximum. *Science*, 325(5941), 710–714. <https://doi.org/10.1126/science.1172873>
- Cohen, K. M., & Gibbard, P. (2011). *Global chronostratigraphical correlation table for the last 2.7 million years*. Subcommittee on Quaternary Stratigraphy (International Commission on Stratigraphy), Cambridge, UK.
- Conato, V., Esu, D., Malatesta, A., & Zarlenga, F. (1980). New data on the Pleistocene of Rome. *Quaternaria*, 22, 131–176.
- Corrado, S., Cosentino, D., Crescenzi, B., & Parotto, M. (1992). Geometrie delle deformazioni della Sabina meridionale attraverso la ricostruzione di superfici strutturali (Lazio, Appennino Centrale). *Studi Geologici Camerti*, 1991, 47–53. <http://193.204.8.201:8080/jspui/handle/1336/779>
- Cosentino, D., & Parotto, M. (1986). Assetto strutturale dei Monti Lucretili settentrionali (Sabina): Nuovi dati e schema tettonico pre-eliminar. *Geologica Romana*, 25, 73–90.
- Croci, A., Della Porta, G., & Capezzuoli, E. (2016). Depositional architecture of a mixed travertine-terrigeneous system in a fault-controlled continental extensional basin (Messinian, Southern Tuscany, Central Italy). *Sedimentary Geology*, 332, 13–39. <https://doi.org/10.1016/j.sedgeo.2015.11.007>
- D'Argenio, B., Ferreri, V., & Anzalone, E. (2008). Travertines and carbonate platforms. Geometries and evolutionary trends compared. *Rendiconti Online della Società Geologica Italiana*, 2, 67–72.
- De Filippis, L., Anzalone, E., Billi, A., Faccenna, C., Poncia, P. P., & Sella, P. (2013). The origin and growth of a recently active fissure ridge travertine over a seismic fault, Tivoli, Italy. *Geomorphology*, 195, 13–26. <https://doi.org/10.1016/j.geomorph.2013.04.019>
- De Filippis, L., Faccenna, C., Billi, A., Anzalone, E., Brilli, M., Soligo, M., & Tuccimei, P. (2013). Plateau versus fissure ridge travertines from Quaternary geothermal springs of Italy and Turkey: Interactions and feedbacks between fluid discharge, paleoclimate, and tectonics. *Earth Science Review*, 123, 35–52. <https://doi.org/10.1016/j.earscirev.2013.04.004>
- De Rita, D., Faccenna, C., Funicello, R., & Rosa, C. (1995). Structural and geological evolution of the Colli Albani volcanic district. *Tipografia SGS*, 33–71.
- De Rita, D., Funicello, R., Corda, L., Sposato, A., & Rossi, U. (1993). Volcanic unit. *Monografie Finali*, 11, 33–79.
- De Rita, D., Giordano, G., Esposito, A., Fabbri, M., & Rodani, S. (2002). Large volume phreatomagmatic ignimbrites from the Colli Albani volcano (Middle Pleistocene, Italy). *Journal of Volcanology and Geothermal Research*, 118, 77–98. [https://doi.org/10.1016/S0377-0273\(02\)00251-2](https://doi.org/10.1016/S0377-0273(02)00251-2)
- Della Porta, G. (2015). Carbonate build-ups in lacustrine, hydrothermal and fluvial settings: Comparing depositional geometry, fabric types and geochemical signature. *Geological Society of London, Special Publication*, 418, 17–68. <https://doi.org/10.1144/SP418.4>
- Della Porta, G., Capezzuoli, E., & De Bernardo, A. (2017). Facies character and depositional architecture of hydrothermal travertine slope aprons (Pleistocene, Acquasanta Terme, Central Italy). *Marine and Petroleum Geology*, 87, 171–187. <https://doi.org/10.1016/j.marpetgeo.2017.03.014>
- Della Porta, G., Croci, A., Marini, M., & Kele, S. (2017). Depositional architecture, facies character and geochemical signature of the Tivoli travertines (Pleistocene, Acque Albule Basin, Central Italy). *Rivista Italiana di Paleontologia e Stratigrafia*, 123, 487–540. <https://doi.org/10.13130/2039-4942/9148>
- Di Nezza, M., Cecchini, F., Margottini, S., & Di Filippo, M. (2015). Assetto geologico strutturale profondo del Bacino delle Acque Albule (Roma, Lazio). *Memorie Descrittive della Carta Geologica d'Italia, XCIX*, 267–272.
- Di Salvo, C., Mazza, R., & Capelli, G. (2013). Gli acquiferi in travertino del Lazio: Schemi idrogeologici e caratteristiche chimico-fisiche. *Rendiconti Online della Società Geologica Italiana*, 27, 54–76. <https://doi.org/10.3301/ROL.2013.20>
- Dickinson, W. R. (1993). Basin geodynamics. *Basin Research*, 5, 195–196. <https://doi.org/10.1111/j.1365-2117.1993.tb00066.x>
- Digital Globe. (2018). *Google, 2018. Google Earth/Maps*. <http://www.earth.google.com>
- Emiliani, C. (1955). Pleistocene temperatures. *Journal of Geology*, 63, 538–578. <https://doi.org/10.1086/626295>
- Erthal, M. M., Capezzuoli, E., Mancini, A., Claes, H., Soete, J., & Swennen, R. (2017). Shrub morpho-types as indicator for the water flow energy – Tivoli travertine case (Central Italy). *Sedimentary Geology*, 347, 79–99. <https://doi.org/10.1016/j.sedgeo.2016.11.008>
- Faccenna, C., Funicello, R., Montone, P., Parotto, M., & Voltaggio, M. (1994). Late Pleistocene strike-slip tectonics in the Acque Albule Basin (Tivoli, Latium). *Memorie Descrittive della Carta Geologica d'Italia*, 49, 37–50.
- Faccenna, C., Soligo, M., Billi, A., De Filippis, L., Funicello, R., Rossetti, C., & Tuccimei, P. (2008). Late Pleistocene depositional cycles of the *Lapis Tiburtinus* travertine (Tivoli, Central Italy): Possible influence of climate and fault activity. *Global and Planetary Change*, 63, 299–308. <https://doi.org/10.1016/j.gloplacha.2008.06.006>
- Folk, R. L., Chafetz, H. S., & Tiezzi, P. A. (1985). Bizarre forms of depositional and diagenetic calcite in hot-spring travertines, Central Italy. *SEPM Special Publication*, 36, 349–369.
- Fornaseri, M. (1985). Geochronology of volcanic rocks from Lazio (Italy). *Rendiconti della Società Italiana di Mineralogia e Petrografia*, 40, 73–106.
- Funicello, R., Locardi, E., & Parotto, M. (1976). Lineamenti geologici dell'area sabatina orientale. *Bollettino della Società Geologica Italiana*, 95, 831–849.
- Gaeta, M., Fabrizio, G., & Cavarretta, G. (2000). F-phlogopites in the Alban Hills Volcanic District (Central Italy): Indications regarding the role of volatiles in magmatic crystallisation. *Journal of Volcanology and Geothermal Research*, 99, 179–193. [https://doi.org/10.1016/S0377-0273\(00\)00172-4](https://doi.org/10.1016/S0377-0273(00)00172-4)

- Gandin, A., & Capezuoli, E. (2014). Travertine: Distinctive depositional fabrics of carbonates from thermal spring systems. *Sedimentology*, *61*, 264–290. <https://doi.org/10.1111/sed.12087>
- Gasparini, C., Di Maro, R., Pagliuca, N., Pirro, M., & Marchetti, A. (2002). Recent seismicity of the 'Acque Albule' travertine basin. *Annals of Geophysics*, *45*, 537–550.
- Giustini, F., Brilli, M., Di Salvo, C., Mancini, M., & Voltaggio, M. (2020). Multidisciplinary characterization of the buried travertine body of Prima Porta (Central Italy). *Quaternary International*, *568*, 65–78. <https://doi.org/10.1016/j.quaint.2020.10.062>
- Guo, L., & Riding, R. (1994). Origin and diagenesis of Quaternary travertine shrub fabrics, Rapolano Terme, Central Italy. *Sedimentology*, *41*, 499–520. <https://doi.org/10.1111/j.1365-3091.1994.tb02008.x>
- Guo, L., & Riding, R. (1998). Hot-spring travertine facies and sequences, Late Pleistocene, Rapolano Terme, Italy. *Sedimentology*, *45*, 163–180. <https://doi.org/10.1046/j.1365-3091.1998.00141.x>
- Guo, L., & Riding, R. (1999). Rapid facies changes in Holocene fissure ridge hot spring travertines, Rapolano Terme, Italy. *Sedimentology*, *46*, 1145–1158. <https://doi.org/10.1046/j.1365-3091.1999.00269.x>
- Hancock, P. L., Chalmers, R. M. L., Altunel, E., & Çakir, Z. (1999). Travertines: Using travertine in active fault studies. *Journal of Structural Geology*, *21*, 903–916. [https://doi.org/10.1016/S0191-8141\(99\)00061-9](https://doi.org/10.1016/S0191-8141(99)00061-9)
- Janssens, N., Capezuoli, E., Claes, H., Muchez, P., Yu, T. L., Shen, C.-C., Ellam, R. M., & Swennen, R. (2020). Fossil travertine system and its palaeofluid provenance, migration and evolution through time: Example from the geothermal area of Acquasanta Terme (Central Italy). *Sedimentary Geology*, *398*, 105580. <https://doi.org/10.1016/j.sedgeo.2019.105580>
- Jones, B., & Renaut, R. W. (1995). Noncrystallographic calcite dendrites from hot-spring deposits at Lake Bogoria, Kenya. *Journal of Sedimentary Research*, *65*, 154–169.
- Karner, D. B., Marra, F., & Renne, P. R. (2001). The history of the Monti Sabatini and Alban Hills volcanoes: Groundwork for assessing volcanic-tectonic hazards for Rome. *Journal of Volcanology and Geothermal Research*, *107*, 185–219. [https://doi.org/10.1016/S0377-0273\(00\)00258-4](https://doi.org/10.1016/S0377-0273(00)00258-4)
- La Vigna, F., Mazza, R., & Capelli, G. (2013a). Water resources in the travertines of Tivoli-Guidonia plain. Numerical modeling as a tool for aquifer management. Le risorse idriche nei travertini della piana di Tivoli-Guidonia. La modellazione numerica come strumento di gestione degli acquiferi. *Rendiconti Online della Società Geologica Italiana*, *27*, 77–85. <https://doi.org/10.3301/ROL.2013.21>
- La Vigna, F., Mazza, R., & Capelli, G. (2013b). Detecting the flow relationships between deep and shallow aquifers in an exploited groundwater system, using long-term monitoring data and quantitative hydrogeology: The Acque Albule basin case (Rome, Italy). *Hydrological Processes*, *27*, 3159–3173. <https://doi.org/10.1002/hyp.9494>
- Lerche, I. (1990). *Basin analysis: Quantitative methods*. Academic Press. ISBN: 0-12-444173-4.
- Mancini, A., Capezuoli, E., Erthal, M., & Swennen, R. (2019). Hierarchical approach to define travertine depositional systems: 3D conceptual morphological model and possible applications. *Marine and Petroleum Geology*, *103*, 549–563. <https://doi.org/10.1016/j.marpetgeo.2019.02.021>
- Mancini, M., D'Anastasio, E., Barbieri, M., & De Martini, P. M. (2007). Geomorphological, paleontological and  $^{87}\text{Sr}/^{86}\text{Sr}$  isotope analyses of early Pleistocene paleoshorelines to define the uplift of Central Apennines (Italy). *Quaternary Research*, *67*, 487–501. <https://doi.org/10.1016/j.yqres.2007.01.005>
- Mancini, M., Marini, M., Moscatelli, M., Pagliaroli, A., Stigliano, F., Di Salvo, C., Simionato, M., Cavinato, G. P., & Corazza, A. (2014). A physical stratigraphy model for seismic microzonation of the Central Archaeological Area of Rome (Italy). *Bulletin of Earthquake Engineering*, *12*, 1339–1363. <https://doi.org/10.1007/s10518-014-9584-2>
- Martín-Algarra, A., Martín-Martín, M., Andreo, B., Julia, R., & Gonzalez-Gomez, C. (2003). Sedimentary patterns in perched spring travertines near Granada (Spain) as indicators of the paleo-hydrological and paleoclimatological evolution of a karst massif. *Sedimentary Geology*, *161*, 217–228. [https://doi.org/10.1016/S0037-0738\(03\)00115-5](https://doi.org/10.1016/S0037-0738(03)00115-5)
- Milli, S. (1997). Depositional setting and high-frequency sequence stratigraphy of the middle-upper Pleistocene to Holocene deposits of the Roman basin. *Geologica Romana*, *33*, 99–136.
- Milli, S., Mancini, M., Moscatelli, M., Stigliano, F., Marini, M., & Cavinato, G. P. (2016). From river to shelf, anatomy of a high-frequency depositional sequence: The Late Pleistocene to Holocene Tiber depositional sequence. *Sedimentology*, *63*, 1886–1928. <https://doi.org/10.1111/sed.12277>
- Milli, S., Moscatelli, M., Palombo, M. R., Parlagreco, L., & Paciucci, M. (2008). Incised valleys, their filling and mammal fossil record: A case study from Middle-Upper Pleistocene deposits of the Roman Basin (Latium, Italy). *GeoActa Special Publication*, *1*, 67–87.
- Minissale, A. (2004). Origin, transport and discharge of  $\text{CO}_2$  in Central Italy. *Earth Science Review*, *66*, 89–141. <https://doi.org/10.1016/j.earscirev.2003.09.001>
- Minissale, A., Kerrick, D. M., Magro, G., Murrell, M. T., Paladini, M., Rihs, S., Sturchio, N. C., Tassi, F., & Vaselli, O. (2002). Geochemistry of Quaternary travertines in the region north of Rome (Italy): Structural, hydrologic, and paleoclimatic implications. *Earth Planetary Science Letter*, *203*, 709–728. [https://doi.org/10.1016/S0012-821X\(02\)00875-0](https://doi.org/10.1016/S0012-821X(02)00875-0)
- North American Commission on Stratigraphic Nomenclature (NACSN). (1983). North American stratigraphic code. *American Association of Petroleum Geologists Bulletin*, *67*, 841–875.
- Özkul, M., Kele, S., Gökgöz, A., Shen, C. C., Jones, B., Baykara, M. O., Föziz, I., Németh, T., Chang, Y. W., & Alçiçek, M. C. (2013). Comparison of the Quaternary travertine sites in the Denizli extensional basin based on their depositional and geochemical data. *Sedimentary Geology*, *294*, 179–204. <https://doi.org/10.1016/j.sedgeo.2013.05.018>
- Patacca, E., Sartori, R., & Scandone, P. (1992). Tyrrhenian basin and Apenninic arcs: Kinematic relations since late Tortonian times. *Memorie della Società Geologica Italiana*, *45*, 425–451.
- Peccerillo, A. (2005). *Plio-quaternary volcanism in Italy. Petrology, geochemistry, geodynamics*. Springer, Heidelberg. ISBN: 978-3-540-29092-6.
- Pedley, H. M. (1990). Classification and environmental models of cool freshwater tufas. *Sedimentary Geology*, *68*, 143–154. [https://doi.org/10.1016/0037-0738\(90\)90124-C](https://doi.org/10.1016/0037-0738(90)90124-C)
- Pentecost, A. (2005). *Travertine*. Springer, Heidelberg. ISBN: 1 4020 3523 3.
- Pentecost, A., & Tortora, C. (1989). Bagni di Tivoli, Lazio: A modern travertine depositing site and its associated microorganisms. *Bollettino della Società Geologica Italiana*, *108*, 315–324.

- Rainey, D. K., & Jones, B. (2009). Abiotic versus biotic controls on the development of the Fairmont Hot Springs carbonate deposit, British Columbia, Canada. *Sedimentology*, *56*, 1832–1857. <https://doi.org/10.1111/j.1365-3091.2009.01059.x>
- Rossetti, F., Tecce, F., Billi, A., & Brilli, M. (2007). Patterns of fluid flow in the contact aureole of the late Miocene Monte Capanne pluton (Elba Island, Italy): The role of structures and rheology. *Contributions to Mineralogy and Petrology*, *153*, 743–760. <https://doi.org/10.1007/s00410-006-0175-3>
- Salvati, R., & Sasowsky, I. D. (2002). Development of collapse sinkhole in areas of groundwater discharge. *Journal of Hydrology*, *264*, 1–11. [https://doi.org/10.1016/S0022-1694\(02\)00062-8](https://doi.org/10.1016/S0022-1694(02)00062-8)
- Shackleton, N. J. (1969). The last interglacial in the marine and terrestrial record. *Proceedings of the Royal Society of London, B*, *174*, 135–154.
- Shiraishi, F., Morikawa, A., Kuroshima, K., Amekawa, S., Yu, T.-L., Shen, C.-C., Kakizaki, Y., Kano, A., Asada, J., & Bahniuk, A. M. (2020). Genesis and diagenesis of travertine, Futamata hot spring, Japan. *Sedimentary Geology*, *405*, 105706. <https://doi.org/10.1016/j.sedgeo.2020.105706>
- Uysal, I. T., Feng, Y., Zhao, J. X., Isik, V., Nuriel, P., & Golding, S. D. (2009). Hydrothermal CO<sub>2</sub> degassing in seismically active zones during the Late Quaternary. *Chemical Geology*, *265*, 442–454. <https://doi.org/10.1016/j.chemgeo.2009.05.011>
- Van Noten, K., Claes, H., Soete, J., Foubert, A., Özkul, M., & Swennen, R. (2013). Fracture networks and strike–slip deformation along reactivated normal faults in Quaternary travertine deposits, Denizli Basin, western Turkey. *Tectonophysics*, *588*, 154–170. <http://dx.doi.org/10.1016/j.tecto.2012.12.018>
- Vignaroli, G., Mancini, M., Bucci, F., Cardinali, M., Cavinato, G. P., Moscatelli, M., Putignano, M. L., Sirianni, P., Santangelo, M., Ardizzone, F., Cosentino, G., Di Salvo, C., Fiorucci, F., Gaudiosi, I., Giallini, S., Messina, P., Peronace, F., Polpetta, P., Reichenbach, V., ... Stigliano, F. (2019). Geology of the central part of the Amatrice Basin (Central Apennines, Italy). *Journal of Maps*, *15*(2), 193–202. <https://doi.org/10.1080/17445647.2019.1570877>
- Waelbroeck, C., Labeyrie, L., Michel, E., Duplessy, J. C., McManus, J. F., Lambeck, K., Balbon, E., & Labracherie, M. (2002). Sea-level and deep water temperature changes derived from benthic foraminifera isotopic records. *Quaternary Science Reviews*, *21*, 295–305. [https://doi.org/10.1016/S0277-3791\(01\)00101-9](https://doi.org/10.1016/S0277-3791(01)00101-9)

## SUPPORTING INFORMATION

Additional Supporting Information may be found online in the Supporting Information section.

**How to cite this article:** Mancini A, Della Porta G, Swennen R, Capezzuoli E. 3D reconstruction of the *Lapis Tiburtinus* (Tivoli, Central Italy): The control of climatic and sea-level changes on travertine deposition. *Basin Res.* 2021;00:1–31. <https://doi.org/10.1111/bre.12576>